(2)

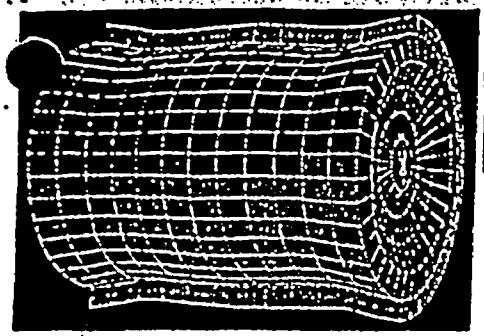

Modelling CANDU Fuel under Normal Operating Conditions:

ELESTRES Code Description

by M. Tayal

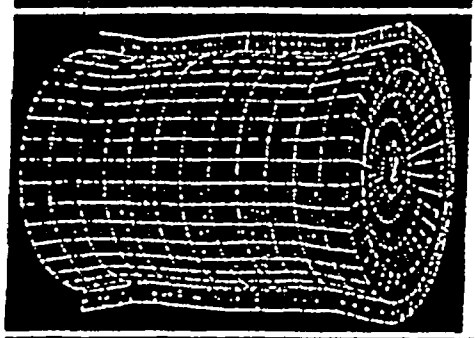

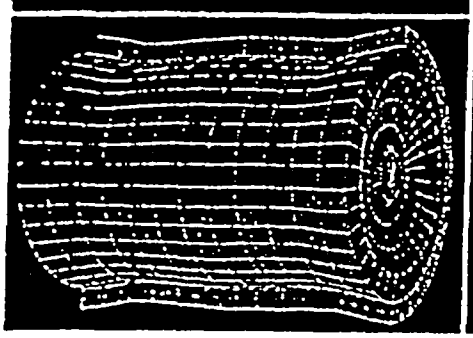

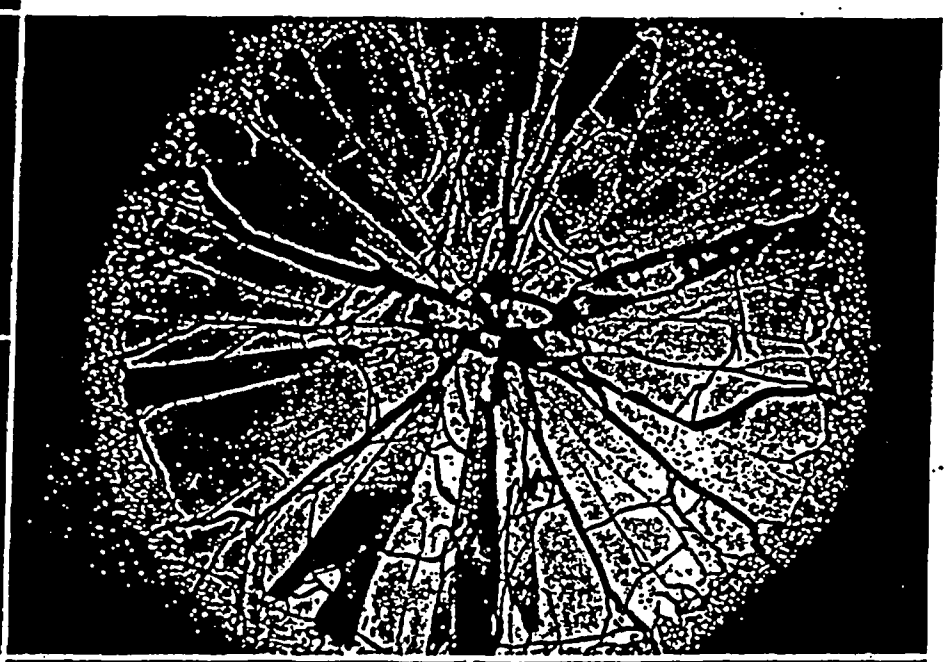

February 1987

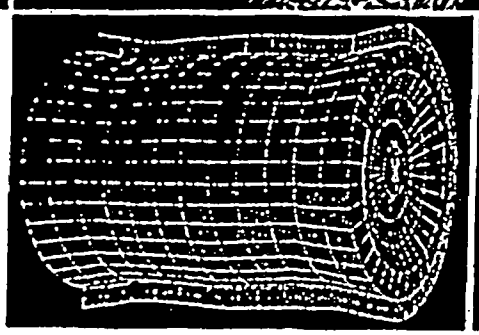

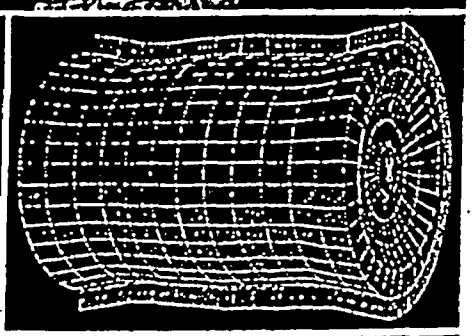

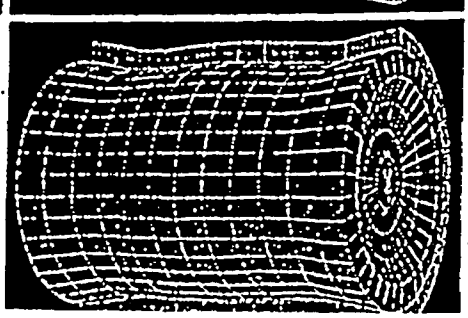

CANDEV-86-110
AECL-9331

Modelling CANDU Fuel Under Normal Operating Conditions: ELESTRES Code Description

by M. Tayal

ABSTRACT

In nuclear fuel elements, sheaths provide a barrier against release of radioactive fission products to the surrounding coolant. Hence the integrity of the sheath and of the sheath/endcap weld, is an important consideration in the design of fuel elements.

The finite element code ELESTRES models the two-dimensional axisymmetric behaviour of a CANDU fuel element during normal operating conditions such as steady power, power changes, and load following. The main focus of the code is to estimate temperatures, fission gas release, and axial variations of deformations/stresses in the pellet and in the sheath. Thus the code models details like stresses/strains at circumferential ridges.

This report describes the major features of an improved version of ELESTRES.

Predictions of ELESTRES show good agreement with about 80 measurements of fission gas release. In this report, we also present ELESTRES predictions of hoop strains in sheaths, for two irradiations. For both irradiations, predictions compare favourably with measurements. An illustrative example shows that near circumferential ridges, bending contributes to multiaxial stresses in the sheath. This can have a significant effect on sheath integrity, such as during stress corrosion cracking due to power increases, or during corrosion-assisted-fatigue due to power-cycling.

Modélisation du combustible du CANDU dans des conditions de fonctionnement normales : description du code ELESTRES

par M. Tayal

RÉSUMÉ

Les gaines des éléments combustibles nucléaires constituent une barrière contre la libération de produits de fission radioactifs dans le caloporteur qui les entoure. Il faut donc accorder une grande importance à l'intégrité de la soudure entre la gaine et le bouchon d'élément au moment de la conception des éléments combustibles.

Le code à éléments finis ELESTRES modélise le comportement axisymétrique bidimensionnel d'un élément combustible du CANDU, dans des conditions de fonctionnement normales, comme une puissance constante, des changements de puissance ou le suivi de charge. La principale fonction du code est d'évaluer la température, la libération des gaz de fission et les variations axiales de déformations et de contraintes dans la pastille et dans la gaine. Ainsi, le code modélise des détails tels que les contraintes et les déformations survenues à la circonférence.

Le présent rapport décrit les principales caractéristiques d'une version améliorée d'ELESTRES.

Les prévisions d'ELESTRES s'accordent avec à peu près 80 mesures de libération de gaz de fission. Vous trouverez également dans le présent rapport les prévisions d'ELESTRES relativement aux contraintes circonférentielles dans les gaines, pour deux irradiations. Ces prévisions correspondent assez aux mesures, dans les deux cas cités. Un exemple graphique démontre que, près de la circonférence, la flexion augmente les contraintes multiaxiales dans la gaine, ce qui peut avoir un effet notable sur l'intégrité de la gaine, comme durant la fissuration par corrosion sous tension causée par l'augmentation de la puissance, ou encore pendant la fatigue avec corrosion due au cyclage.

Atomic Energy of Canada Limited
CANDU Operations

L'Énergie Atomique du Canada, Limitée
Opérations CANDU

CANDEV-86-110
AECL-9331

Sheridan Park Research Community
Mississauga, Ontario L5K 1B2
Tel. (416) 823-9040

Table of Contents

List of Figures and Tables

Modelling CANDU Fuel Under Normal Operating Conditions: ELESTRES Code Description

by

H. Tayal

1. INTRODUCTION

1.1 Need

A nuclear fuel element consists of a cylindrical tube containing sintered uranium dioxide pellets. The tube, called the sheath, is sealed at the two ends by welds to the endcaps. The sheath provides a barrier against release of radioactive fission products to the surrounding coolant. Hence, the integrity of the sheath and of the sheath/endcap weld, is an important consideration in the design of fuel elements.

In the reactor, the pellet heats up and expands, potentially pushing the sheath and the endcap. The resulting stresses can combine with chemical/metallurgical effects such as corrosion from fission products like iodine/cesium, with embrittlement due to hydrides/deuterides, and with embrittlement due to irradiation. These combinations are important contributors [1] to potential failures during normal operating conditions such as power ramps, load following, and even long steady powers.

The computer code ELESTRES* models [2] the thermal and mechanical behaviour of an individual fuel element, during its irradiation life under normal operating conditions. A recent paper [3] briefly described the current version of the code. This report describes ELESTRES in more detail.

This report first lists the applicability of ELESTRES, summarizes its evolution and then describes the physical models in ELESTRES and how they are linked. Details of the major features of the code, followed by some comparisons of predictions to measurements, are given. Finally, two specific applications are discussed.

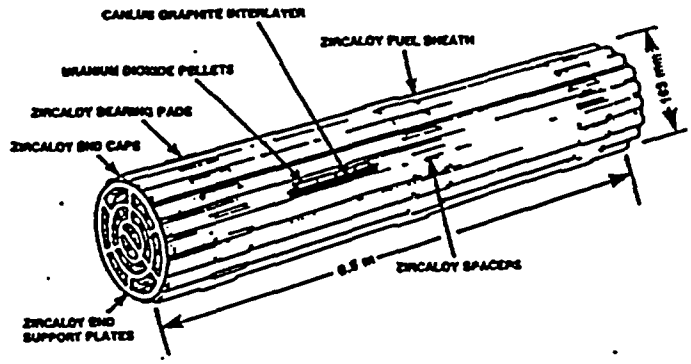

Figure 1 Fuel Bundle

1.2 Definitions

Figure 1 shows the geometry of a CANDU** fuel bundle. Figure 2 shows a fuel element. The two figures also illustrate some terms relevant to this report. The bundle contains 20–40 fuel elements. Each element has one sheath made of Zircaloy-4. Each sheath contains 20–40 pellets of UO_2, which produce heat in the reactor. Reference 4 describes the fuel bundle in more detail.

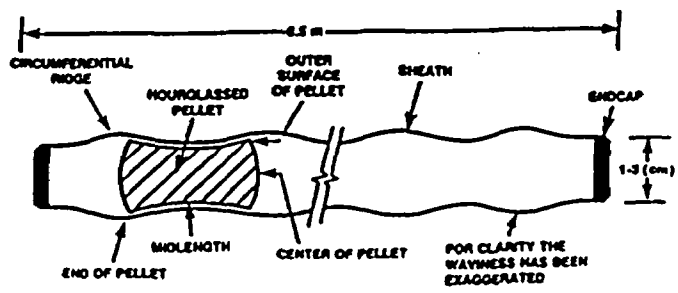

Figure 2 Fuel Element

* ELESTRES: ELEment Simulation and sTRESses

** CANDU – CANada Deuterium Uranium – is a registered trademark of Atomic Energy of

Figure 3a shows measurements [5] of sheath diameter after an irradiation at Chalk River Nuclear Laboratories. The sheath diameter, and strain, are larger at interfaces of neighbouring pellets than at midplanes of pellets. The larger strain at pellet interface is called a circumferential ridge. It is a result of axially - non-uniform, radial expansion of the pellet. In Figure 3a, the permanent hoop strain at the ridge is 1.7% - well into the plastic range. Figure 3b shows a calculated shape of the pellet and the sheath, during initial rise to power.

1.3 Applications

The following are the main parameters calculated by ELESTRES:

(i) Temperature along the radius of the pellet and the sheath.

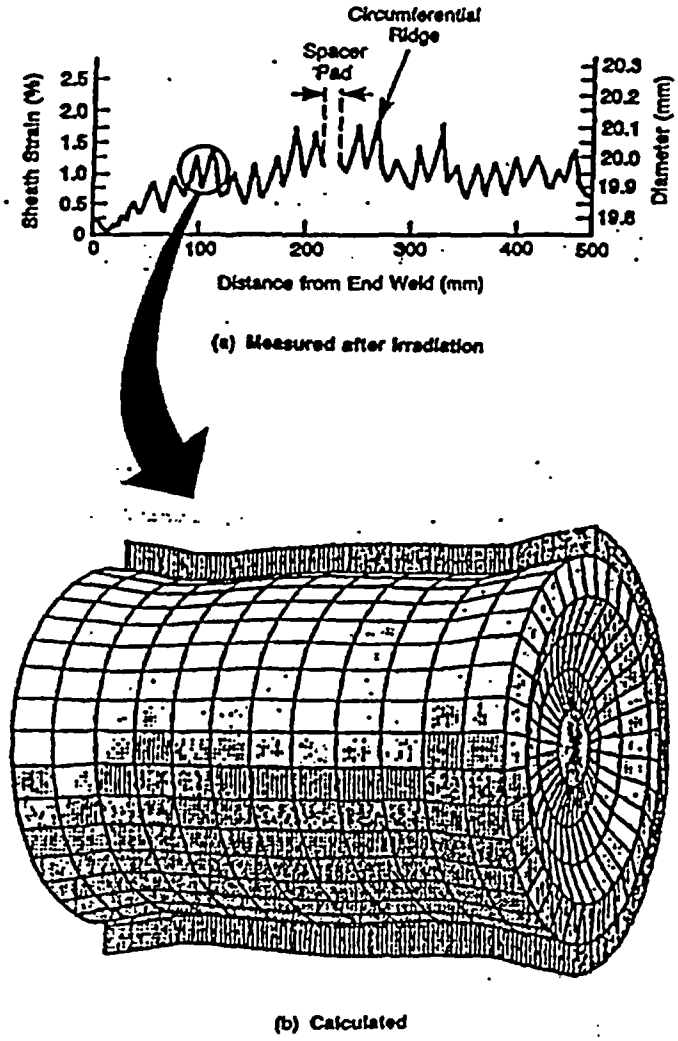

Figure 3 Circumferential Ridging and Hourglassing: Measured and Calculated

(ii) Fission gas release and the associated internal gas pressure.

(iii) Strains at and near circumferential ridges.

(iv) Probability of sheath failure due to stress corrosion cracking.

Strains should be kept low to avoid rupturing the sheath. High strains can also lead to channelling [6] of dislocations. Channelling can anneal the hardening due to irradiation. If this occurs at a localized spot, e.g. at circumferential ridges, then a weak spot is created in the sheath. Subsequent strains due to, say fission gas, can then concentrate at the weak spot, rendering the sheath more prone to failure.

Expansion of the pellet is a major source of stresses and strains in sheaths, and in sheath/endcap welds. Stresses should be kept low to avoid failure by stress corrosion cracking.

Stress corrosion cracking may occur due to the combined effects of: (a) stresses due to power increase, and (b) corrodants in the fission products. ELESTRES includes an estimate for the probability of fuel failure due to stress corrosion cracking, based on an empirical correlation.

One application of ELESTRES is to evaluate the ability of a given fuel design to survive the intended environment (e.g. power, burnup) during normal operation. This is done by calculating temperatures to check for melting, by calculating internal pressure to check for bursting, and by calculating ridge strains and stresses to check for the possibility of stress corrosion cracking.

Other applications include: calculating fission gas release as initial conditions for subsequent analyses of sheath strain during hypothetical accidents; and calculating pellet expansion for subsequent use in assessments of stresses near welds between sheaths and endcaps. For these applications, ELESTRES is frequently linked to other codes like FEAST [7], ELOCA [8], and ELOCA-A [9], see Figure 4.

The following are some specific previous applications of ELESTRES:

- Determine the impact of the following parameters, on fuel performance: pellet density; surface roughness; shape and length of the pellet. Figure 5 shows an application of ELESTRES, for studying how ridge strains can be reduced by chamfers and by shorter pellets. The predicted trends agree with Carter's irradiations [10].

- Calculate the power that can cause central melting during normal operation.

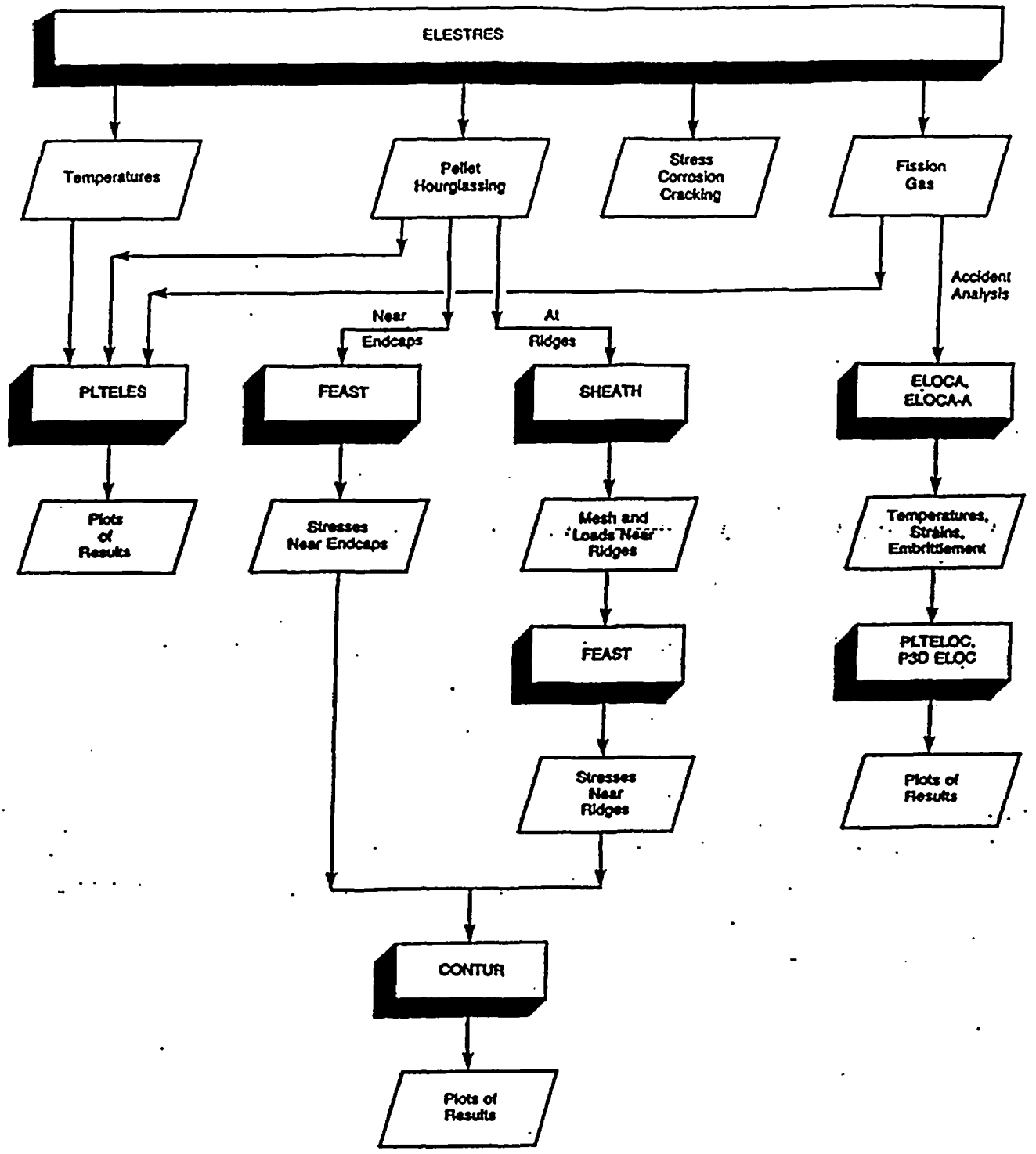

Figure 4 Links between ELESTRES and Related Codes

- Determine the pattern of multiaxial stresses and strains near circumferential ridges.
- Assess the impact of power cycling, on fatigue of the sheath near circumferential ridges. The fatigue may be assisted by corrosion from fission products.
- Assess the pattern of stresses near sheath/endcap welds, in an effort to identify and remove the cause of fuel failures [1] in the Bruce reactor.
- Determine the acceptable distribution of unbonded areas in endcap welds.

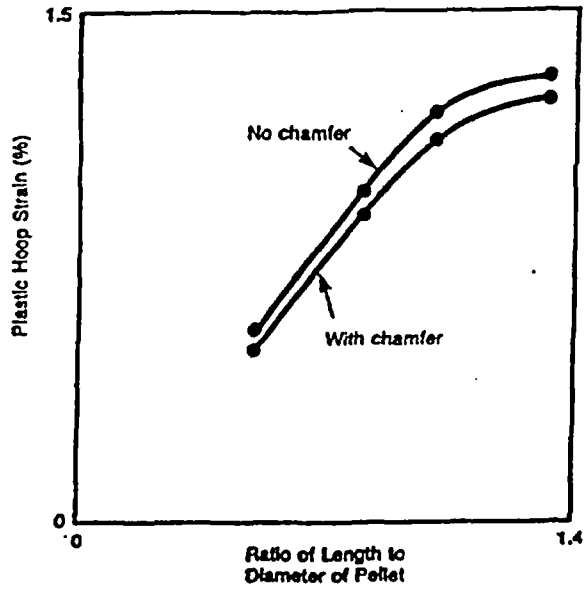

Figure 5 Strain at Ridge: Effect of Pellet Geometry

- Predict the performance of fuel during hypothetical transients involving: Loss of Reactivity Control; Loss of Main Feedwater; and Loss of Coolant. In Figure 6, ELESTRES shows that the gas pressure can be kept below the coolant pressure, during a Loss of Reactivity Control.

- Predict the probability of fuel failure, during multiple ramps in power.

- Calculate temperatures during refuelling. Figure 7 shows the temperatures predicted by ELESTRES, for a fuel element that first resides in a low power position in the channel, then is shifted to a higher power. During the initial irradiation at the low power, densification of UO_2 results in higher thermal conductivity, which reduces the pellet temperature. The shift at 80 MW.h/kgU results in much higher pellet temperature, and in a higher rate of densification.

  Reference 11 discusses some of the above applications.

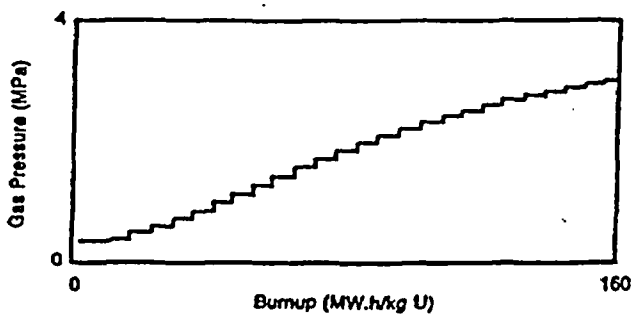

Figure 6 Gas Pressure during a Loss of Control of Reactivity

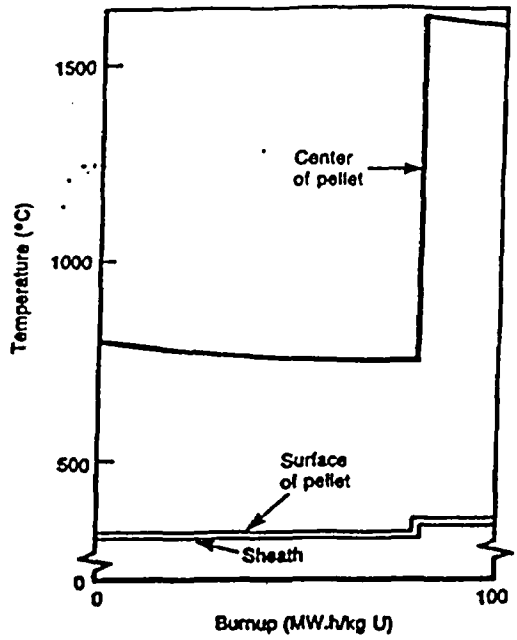

Figure 7 Temperatures During Refuelling

1.4 Features and Evolution

Before we describe the details of ELESTRES, we give a summary of its predecessor, ELESIM [12, 13, 14].

Over the years, ELESIM has been frequently used for modelling the performance of CANDU fuel during normal operation. Its constituent models are physically (rather than empirically) based, and include such phenomena as:

- heat transfer between the pellet and the sheath;
- densification of UO_2 as a function of time and temperature;
- influence of temperature, and of changes in porosity/density, on the thermal conductivity of the pellet;
- effect of burnup on the radial distribution of neutron flux;
- equiaxed and columnar grain growth in the pellet;
- fission gas release as a function of microstructure and of irradiation;
- swelling of UO_2 due to fission products;
- creep of the sheath as a function of stress, of temperature, and of neutron-dose.

ELESIM has been verified [14] extensively against numerous irradiations in experimental and in commercial reactors.

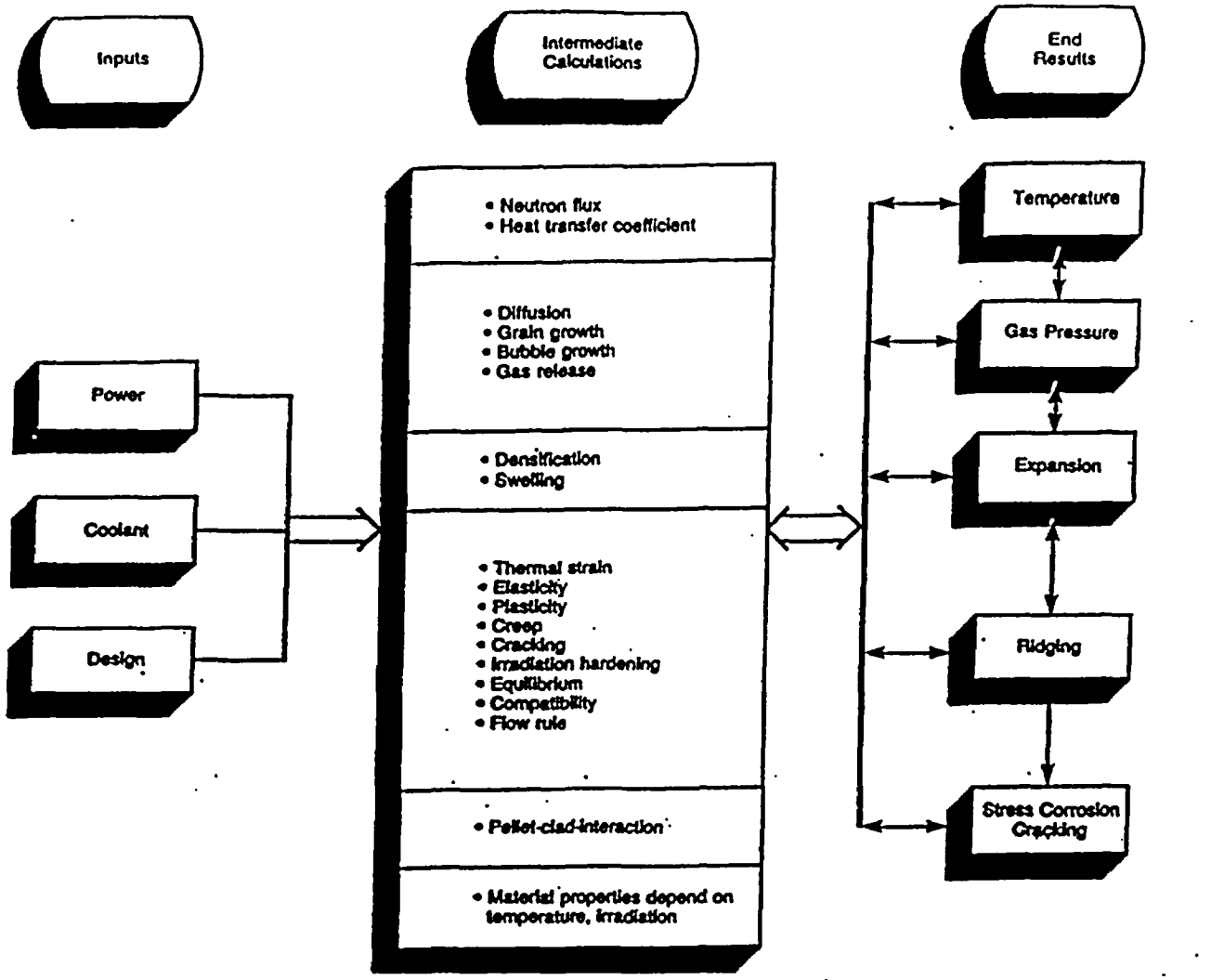

Figure 8 Major Calculations in ELESTRES

ELESTRES retains all the preceding sub-models of ELESIM. In addition, ELESTRES also calculates the deformation of the pellet, by a two-dimensional, axisymmetric, finite element model. The calculations include the effects of thermal, elastic, plastic, and creep strains. Cracking is also simulated. The pellet calculations use an earlier version of the FEAST code [7].

ELESTRES continues to provide the information provided by ELESIM, on temperatures and on fission gas release. In addition, ELESTRES also provides information on circumferential ridging, and, to a limited extent, on stress corrosion cracking.

The first version of ELESTRES was introduced in 1977. Reference 13 gives the details of those portions of ELESTRES that are common with ELESIM. Reference 7 describes the details of the finite element model FEAST, whose earlier version was used in ELESTRES to calculate pellet deformations. Reference 2 describes how the two major parts, ELESIM and FEAST, were combined in the initial version of ELESTRES. Reference 11 describes some recent applications of ELESTRES, in design/analysis of CANDU fuel.

Reference 15 describes a counterpart of ELESTRES for Light Water Reactors: the FEMAXI code. Many features are common between ELESTRES and FEMAXI, although some details differ.

The current version of ELESTRES contains improvements over the original, in the following major areas: link to FEAST for detailed calculations of sheath stresses; yield strength of the pellet; creep rate of Zircaloy; transient temperatures; calculations at end-of-life; ANS 5.4 correlation for gap inventory; densification of UO2; and additional conveniences in input/output/interfacing with other codes. This report describes the significant changes. To provide a perspective, however, we first give an overview of the various physical processes included in ELESTRES. Figure 8 shows how they are linked.

2. CODE OVERVIEW

2.1 Input

ELESTRES assumes that the fuel element consists of a cylindrical tube of Zircaloy or of steel (steel has been used in some experimental fuel), containing a stack of UO_2 pellets. A plenum may also be included. The tube is sealed at both ends. The pellets may be solid or annular, dished or undished, or may be chamfered. The pellets may also contain grooves for instrumentation.

The user specifies the details of the pellet and of the sheath, such as: shapes; dimensions; clearances; density; grain size; surface roughness; type of CANLUB coating; and enrichment. The user also specifies the composition and the pressure of the filling gas. The temperature and the pressure of the coolant are specified as a function of time. The power history is specified in terms of linear heat generation rate vs burnup.

2.2 Calculation Procedure

The power history is divided into a series of increments of powers and burnups. A separate calculation is done for each increment.

An extra set of calculations is done at the end of the specified power history, where the fuel element is assigned a uniform temperature of 20°C. Hence, this calculation gives results that can be compared to post-irradiation measurements.

ELESTRES contains several features that permit large calculation-increments. These include: a special formulation [16] for permitting many finite elements to simultaneously cross the boundary from elastic to plastic behaviour; accommodation of large drops in yield-strength [7] due to changes in local temperature; and a three-step predictor/corrector method for elastic/plastic analyses. These features reduce computing costs. For typical irradiation-histories (powers up to 80 kW/m, burnups up to 300 MW.h/kgU), ELESTRES requires less than one minute of computing time on a CDC/CYBER 175 computer.

2.3 Output

The output of ELESTRES can be controlled by the user, and ranges from one line per calculation, to one page per calculation. Table 1 lists the major parameters printed by ELESTRES. They include: temperatures, fission gas release, displacements, stresses, strains, and defect probabilities.

In addition, ELESTRES stores selected results in three files for future processing, as shown in Figure 4. One file is linked to a routine that plots the results of ELESTRES. Another file preserves pellet deformations. This is used by FEAST to calculate stresses in the sheath near ridges and near endcap welds. The third file contains data needed by ELOCA for accident analyses. Fission gas release is the most important information in this file.

3. THERMAL MODELS

3.1 Neutron Flux

In ELESTRES, the neutron flux is allowed to be non-uniform along the radius of the pellet: it is normally higher near the outer surface, and lower near the center. The radial distribution of neutron flux is a function of pellet diameter, of UO_2 enrichment, and of burnup. ELESTRES also considers the build-up of plutonium near the outer surface of the pellet.

To account for these effects, ELESTRES uses an equation fitted to the results of the neutron-physics code HAMMER [17]. Figure 9 shows

Table 1: Major Outputs of ELESTRES

- Temperatures:
  - Sheath
  - Surface of the pellet
  - Center of the pellet
  - Volume-average in the pellet
- Heat transfer coefficient between the sheath and the pellet
- Fission Gas:
  - percent release
  - free volume
  - pressure
  - isotopic composition
- Interfacial pressure between the pellet and the sheath
- Radial gap between the sheath and the pellet
- Radial and axial deformations of the pellet
- Sheath strain:
  - at the midplane
  - at the end of the pellet
- Stresses in the pellet
- Stresses in the sheath
- Probability of failure due to stress corrosion cracking

a typical distribution of heat generation rate along the radius of the pellet. Near the surface of the pellet, build-up of fissile plutonium gives a sharp increase in the heat generation rate.

3.2 Heat Transfer Coefficient

ELESTRES assumes that the heat transfer coefficient between the sheath and the pellet is a function of:

- radial gap/contact-pressure between the pellet and the sheath;
- the composition of gases inside the fuel element; and
- the initial roughnesses of the surfaces of the sheath and of the pellet.

ELESTRES allows the first two parameters above to change continuously during irradiation. For example, the pellet first expands thermally, then shrinks due to densification, then swells due to solid fission products (discussed later). The sheath creeps due to coolant pressure. Thus the diametral clearance/contact-pressure, between the pellet and the sheath, changes continuously, not only for the preceding reasons, but also due to changes in power. As more fission gases are released from the pellet, the composition of gas changes inside the fuel element. All these effects combine to give a complex variation of heat transfer coefficient between the pellet and the sheath, during the residence of fuel in the reactor.

ELESTRES will predict the resulting changes in the heat transfer coefficient, using the empirical model by Campbell, Borque, Deshaies, Sills, and Notley [18].

Figure 10 shows an illustrative prediction of heat transfer coefficient during an irradiation. Initially, pellet expansion creates a high interfacial pressure between the pellet and the sheath. This gives a high heat transfer coefficient. Then, over the first 100 MW.h/kgU, stress relaxation causes a rapid drop in contact pressure. This decreases the heat transfer coefficient. By then, fission gases accumulate to become a significant fraction of the internal gases, causing further decreases in the heat transfer coefficient. By 200 MW.h/kgU, the contact pressure and the initial filling gas are playing an insignificant role in determining the heat transfer coefficient.

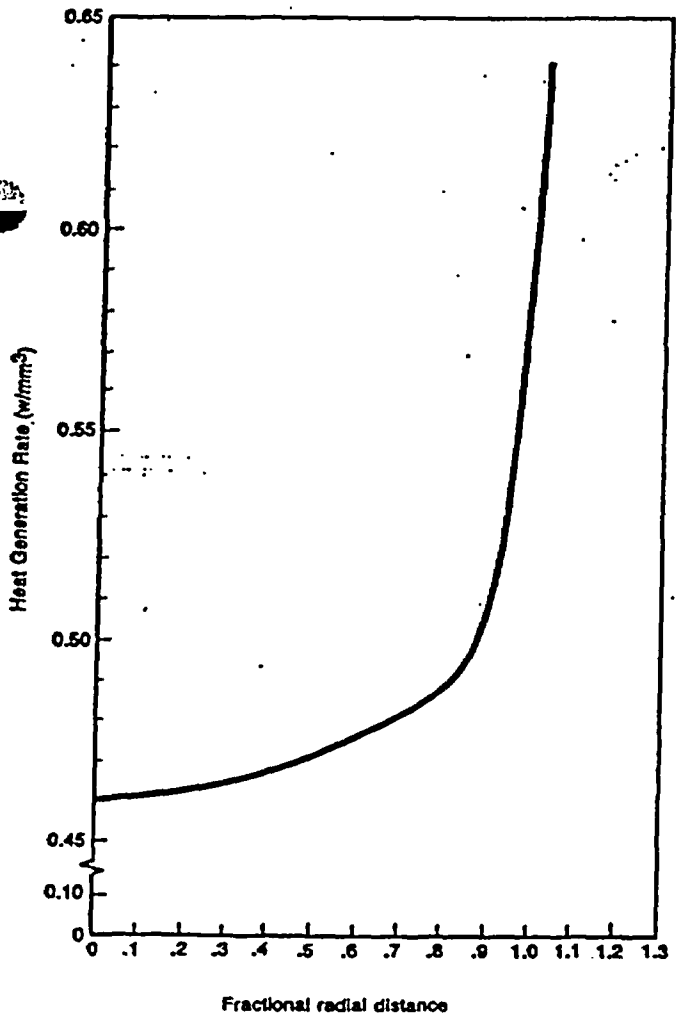

Figure 9 Illustrative profile of heat generation rate across the pellet radius

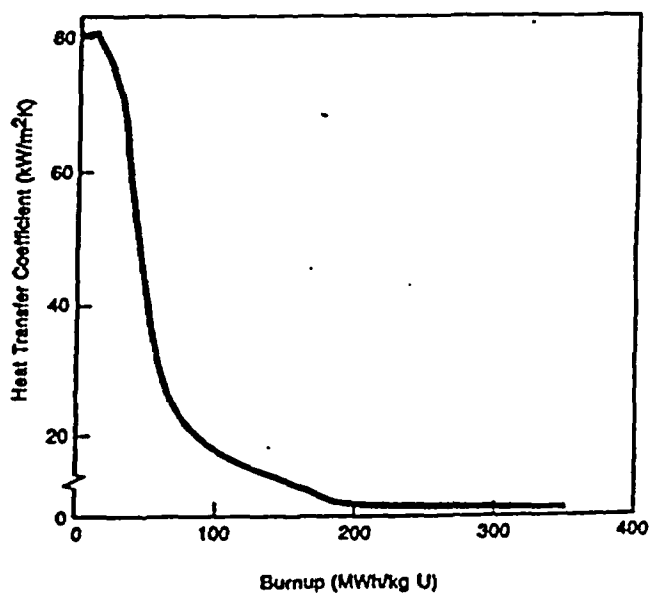

Figure 10 Illustrative variation of heat transfer coefficient (between pellet/sheath)

3.3 Temperature

The temperature in the pellet is normally highest at the center, and lowest near the pellet/sheath interface. Figure 11 shows a typical distribution of temperature.

The code assumes uniform neutron flux along the length of the pellet. Thus, end flux peaking is not considered explicitly. It is, however, considered implicitly, via normalization of predicted gas release to measured (discussed later). In any case, since end flux peaking affects only 5% of the stack length [19], it likely does not contribute significantly to the total gas released in the fuel element.

Two-dimensional calculations using the FULMOD code [20] showed [21] that except for end flux peaking, axial variations in temperature are low: less than 20°C along the length of an individual pellet. These are insignificant compared to the normal temperatures in the pellet: ~ 1800°C at the center. Grain growths measured [22, 23] in the pellets after numerous irradiations also show no axial variations along pellet length, confirming that axial heat conduction is not significant. Therefore, for temperatures, one-dimensional calculations are done in ELESTRES. That is, heat flow is considered along the radial direction, but not along the length, nor around the circumference.

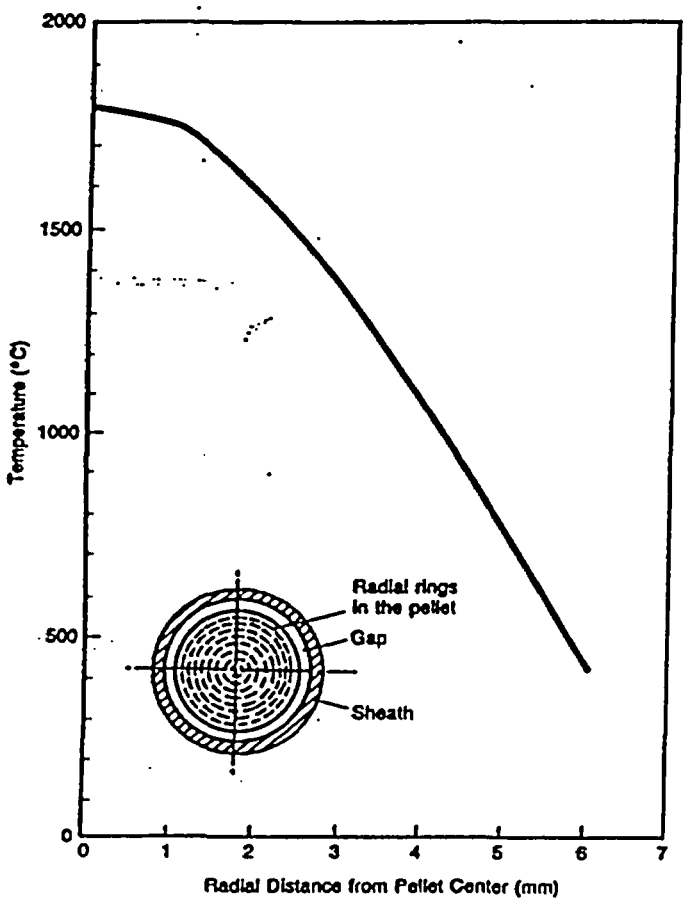

Figure 11 Illustrative Profile of Temperatures in the Pellet

The following classical equation describes transient conduction of heat [24]:

$$k \frac{\partial^2 T}{\partial r^2} + \frac{k}{r} \frac{\partial T}{\partial r} + w = \rho s \frac{\partial T}{\partial t}$$

Here, k is thermal conductivity, T temperature, r radial distance, w rate of heat generation per unit volume, ρ density, s specific heat, and t time.

The above equation is solved [2] using the finite difference method.

The transient effects are important for some short-term situations, e.g. for postulated accidents involving loss of control of reactivity. For these, the full equation above is solved.

For the majority of normal operating conditions, however, the fuel power is usually held constant for a long time, say for more than one hour. This is significantly longer than the thermal time-constant of the fuel element: about 9 s for volume-average temperature, and 11 s at the center of the pellet. For these conditions, ELESTRES saves on computing cost by bypassing the transient calculations, and solving directly for steady-state [2].

Figure 12 shows the thermal conductivity of UO_2, obtained from MATPRO [25]. MATPRO does not refer to the effect of irradiation on the thermal conductivity of UO_2. Reference 26 shows, however, that at low temperatures, the thermal conductivity is also a function of the number of fissions and of the temperature at which the fission damage accumulated. ELESTRES simulates the low temperature damage by assuming that the conductivity is constant below 454°C.

Figure 12 shows that at operating temperatures, the thermal conductivity of UO_2 varies by about a factor of 2. This makes the above equation non-linear.

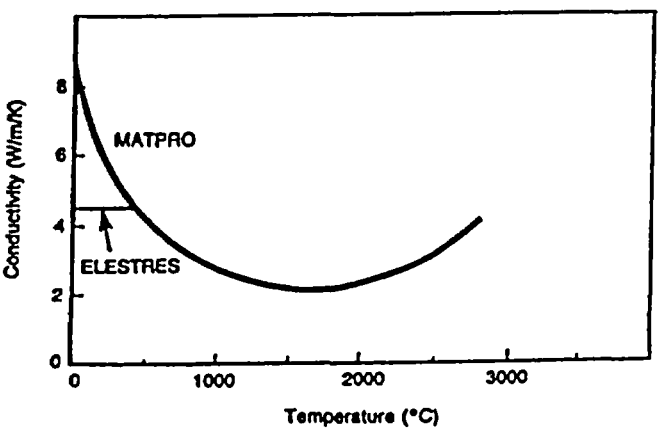

Figure 12 Thermal Conductivity of UO_2

The equation is solved by dividing the pellet into a number of concentric annuli, usually 100, see Figure 11. Another annulus represents the sheath, and one annulus models the gap between the sheath and the pellet. Within each annulus, the temperature is assumed to vary parabolically with distance.

An implicit, incremental formulation of the above equation is obtained by using the one-step, Euler, backward-difference formula [24]. The incremental equations are first formulated for each annulus, then assembled into a matrix to represent all the annuli simultaneously. This system of non-linear equations is solved iteratively, employing the modified Newton-Raphson scheme. The iterations continue until the net flow of heat has a low residual error at each time-step.

4. FISSION GAS

4.1 Grain Growth

High temperatures promote diffusion of UO2 atoms to and along grain boundaries. This results in grain growth [22, 23], equiaxed and columnar. Figure 13 shows some examples.

For equiaxed growth, ELESTRES uses the model by Hastings, Scoberg, and Mackenzie [22]. This empirical model gives the rate of grain growth as a function of: local temperature; enrichment; and the diameter of UO_2.

Columnar grains have been observed [23] in some experimental fuel irradiated at high powers. Columnar grain growth occurs by bubble movement in a thermal gradient. This can occur

(a) Grains in As-sintered Pellets

(b) Equiaxed Grains in Irradiated Pellets

(c) Columnar Grains in Irradiated Pellets

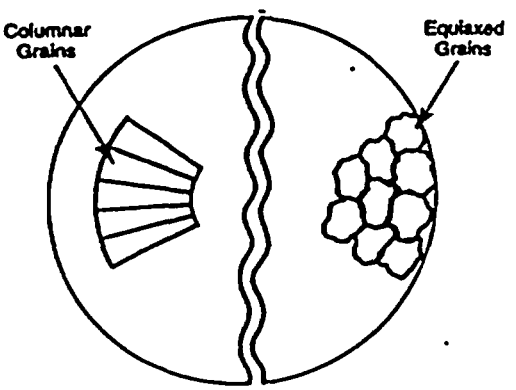

(d) Grain Growth Assumed in ELESTRES

Figure 13 Microstructures in UO_2 Pellets Irradiated in Canadian reactors [22]

(a) Observed after irradiation [23]

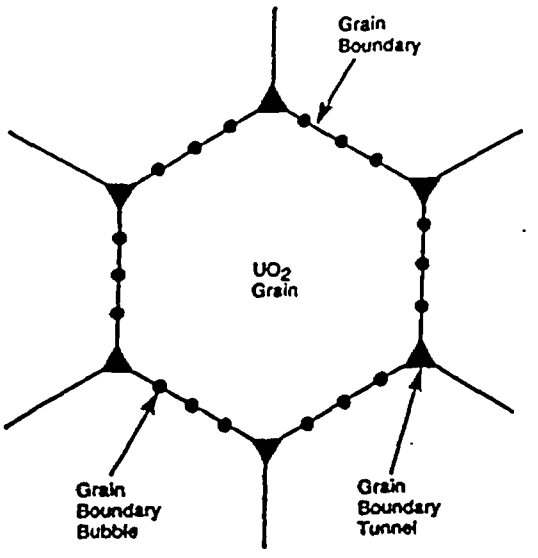

(b) Assumed in ELESTRES

Figure 14 Storage of Fission Gas at Grain Boundaries

by surface diffusion, by volume diffusion, or by vapour phase transport [27]. The ELESTRES model is taken from Reference 14, which is based on a logarithmic average between the rates for surface diffusion and for vapour phase transport [28]. The resulting equations provide the rate of growth of columnar grains, as a function of: local temperature and its gradient; pressure within the gas bubble; and radius of the grain.

4.2 Stable Fission Gases

Irradiation generates fission products within the grains of UO_2. Some of the fission products are gaseous. The gas is assumed to diffuse through UO_2 grains; ELESTRES uses Booth's 'equivalent sphere' model [29] for this calculation. The amount of diffusion to grain-boundaries depends, among others, on the local temperature and on the size of the grain.

The diffused gas accumulates in grain-boundary bubbles [14], see Figure 14. The bubbles grow as more gas reaches the grain boundary, either by diffusion or during grain-boundary sweeping due to grain growth (equiaxed and columnar).

ELESTRES assumes that a change in power generates thermal stresses in the pellet. This produces microscopic (and macroscopic) cracks in the pellet. A path, called tunnels, is formed linking the grain-boundaries to the pellet/sheath gap.

When the bubbles grow big enough to touch each other (i.e. to interlink), any excess gas in the bubbles is assumed to be released from the bubbles, via the tunnels, to the pellet/sheath gap. This gas is called the free gas. It is calculated in ELESTRES using the model by Notley and Hastings [14].

4.3 Radioactive Isotopes

ELESTRES also calculates the radioactive isotopes in the free gas, using the ANS 5.4 model [30]. This is an empirical correlation of measurements from a wide range of experiments. It correlates gas release mainly to temperature and to burnup; more details are available from Reference 30.

ELESTRES calculates the free inventories of 59 radioactive isotopes of 19 elements, selected for their relevance to safety analyses and to radiation shielding. Table 2 lists the pertinent isotopes.

For isotopes whose half-lives are greater than one year, ELESTRES uses the ANS model for stable gas release. For the remaining isotopes, fractional release is based on the maximum temperature reached during the last two half-lives of the isotope, accounting for radioactive decay during diffusion.

4.4 Gas Pressure

The gas pressure inside the fuel element depends on: the mass of the gas; the volume available to store this gas; and the temperatures of the storage locations. ELESTRES calculates the gas pressure by using the ideal gas law.

The total mass of the gas is the sum of the free gas discussed earlier, plus the filling gas used during the fabrication of the fuel element.

ELESTRES considers the following locations for storing the gases:

- Axial gaps between neighbouring pellets and between pellets and the endcaps.
- Dishes, chamfers, grooves, and holes in the pellets.
- Cracks in the pellets.
- Surface roughnesses of the sheath and of the pellets.
- Plenums.
- Radial gap between the pellets and the sheath.
- Open porosity.

5. DEFORMATIONS AND STRESSES

5.1 Diametral Changes

The following processes affect the diameter of the pellet and of the sheath: densification; swelling; creep; thermal expansion; and hourglassing.

Densification is caused primarily by irradiation-induced sintering of UO_2 in the reactor. It is calculated in ELESTRES as a function of: initial density of the pellet; local temperature; and time in the reactor. Swelling is caused by solid products of fission, which have a larger volume than the parent material, and by unreleased fission gases. For these calculations, ELESTRES uses the model [31] by Hastings, Fehrenbach, and Hosbons.

Creep due to external coolant pressure decreases the diameter of the sheath. However, outward creep of the sheath can be expected if the internal gas pressure significantly exceeds the coolant pressure. In calculating thermal expansion, melting of UO_2 is also considered.

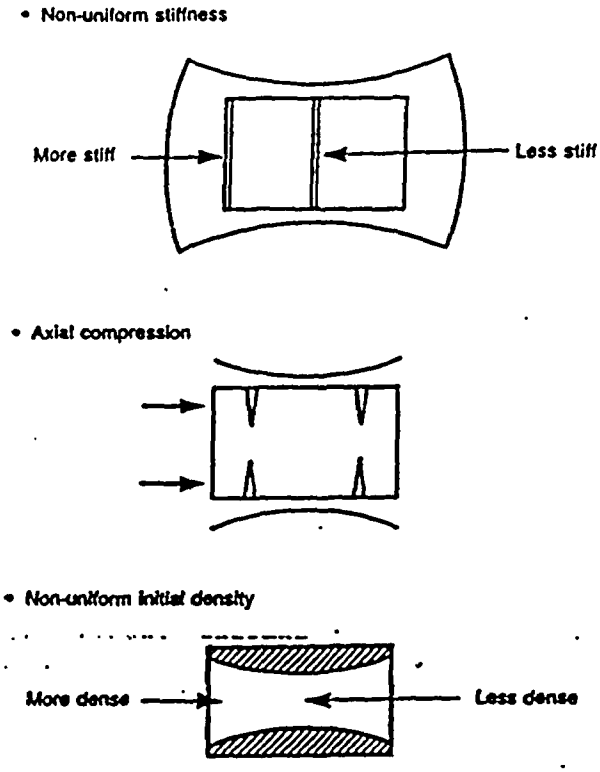

Figure 15 Reasons for Hourglassing of Pellets

5.2 Hourglassing

Hourglassing of the pellets can be caused by three factors: non-uniform temperature along the radius of the pellet; axial compression; and variations in initial density. These are shown schematically in Figure 15.

Table 2: Radioactive Isotopes Considered by ELESTRES

Antimony (128M, 129, 130M, 131)	Praseodymium - 146
Barium (140, 141, 142)	Rubidium (88, 89)
Bromine-84	Ruthenium (103, 106)
Cerium (141, 142)	Strontium (89, 90, 91, 92)
Cesium (137, 138)	Technitium (101, 102)
Iodine (131, 132, 133, 134, 135)	Tellurium (131M, 131, 132, 133M, 133 134, 135)
Krypton (83M, 85M, 85, 87, 88, 89)	Xenon (133M, 133, 135M, 135, 138)
Lanthanum (140, 142, 143)	Yttrium (91M, 94, 95)
Molybdenum (99, 101)	Zirconium (95, 97)
Niobium (95, 97M, 97)	

The temperature profile along the pellet radius is, approximately, parabolic. Hence the thermal expansion does not produce the same radial displacement, nor hoop strain, at adjacent radial locations. The resulting incompatibility causes stresses and strains that change radially and axially. The local strains and stresses are determined by, among others, the local stiffness of the pellet.

At the pellet midplane, the deformation of a transverse cross-section is resisted not only by the stiffness of that cross-section, but also by the stiffness of the neighbouring UO_2. However, near the pellet end, the transverse cross-section is surrounded by less UO_2. Therefore it can, and does, expand more than the cross-section at the pellet midplane, see Figure 3. The pellet thus takes the shape of an hourglass. This is one reason for circumferential ridges.

The amount of hourglassing is affected by many other parameters, for example: the temperature profile; the coolant pressure; the resistance offered by the sheath; the amount of radial interaction between the sheath and the pellet; the amount of cracking in the pellet; the diameter and the length of the pellet; and the sizes of the chamfers, of the lands, and of the dishes at the ends of the pellet.

Axial compression also contributes to hourglassing. When the pellet expands axially, there may be axial interference between neighbouring pellets, and/or between the stack of pellets and the endcap. This causes compressive axial forces on each pellet. Hydraulic drag is another source of compressive axial forces. This adds to the hourglassing of the pellet. Axial compression has a larger influence on ridging if the force is applied near the surface of the pellet than towards the center.

Another contributor to hourglassing is the initial variation of densities in the pellet: higher at the ends, lower at the midplane. Densification in the reactor then leads to hourglassing. This component, however, is presently not considered in ELESTRES.

Veeder presented [32] a polynomial expression for the thermo-elastic hourglassing of the pellet. The solution was obtained by minimizing the strain energy of a right circular finite cylinder.

In ELESTRES, a finite element model is used to calculate the axisymmetric deformation of the pellet [2, 7]. The code models thermal, elastic, plastic, and creep strains and stresses. The code also considers: axial loads; variation of yield strength with temperature; and cracking.

Figure 16 shows that during irradiation, a significant fraction of the pellet can crack. ELESTRES assumes that a radial crack forms when the local tensile hoop stress exceeds the rupture strength. Upon cracking, the previous hoop stress is redistributed to uncracked locations, and no new hoop stress is assigned to the cracked material.

Geometry of the pellet is considered. For example, the code accounts for the length and the diameter of the pellet, and for the sizes of the chamfers/lands/dishes at the ends of the pellet.

The following fundamental laws of mechanics are satisfied: equilibrium; compatibility; constitutive relations; yield criterion; and flow rule.

The preceding calculations employ two-dimensional, axisymmetric calculations. The displacements, stresses, and strains are assumed uniform around the circumference. However, their radial and axial variations are considered.

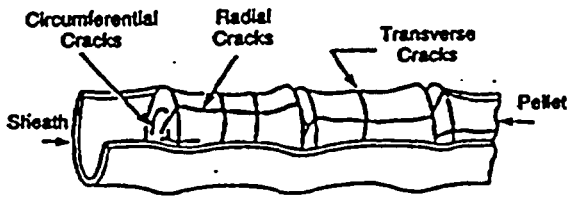

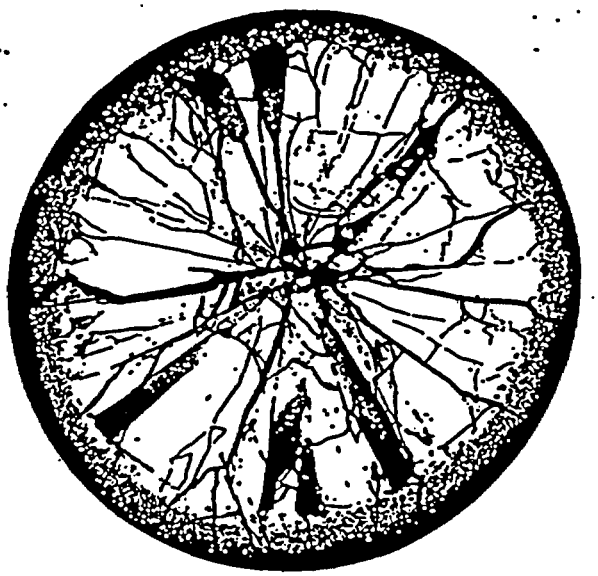

Radial Cracks in a Transverse Section [23]

Figure 16 Possible Cracks in a Pellet

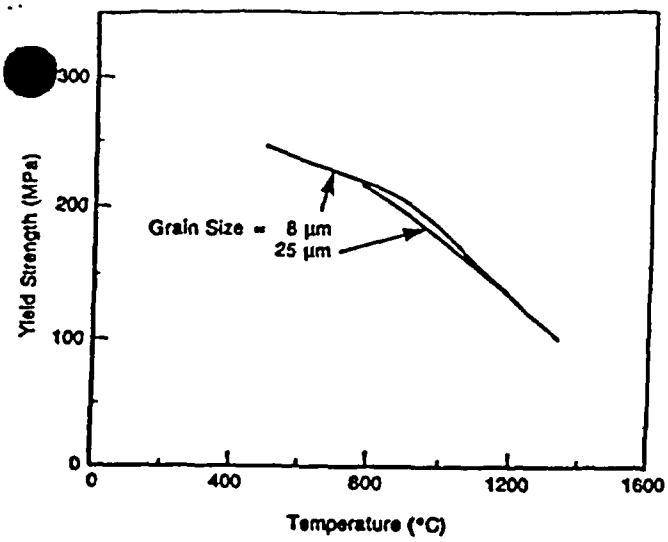

Figure 17 Yield Strength of UO_2 [25]

5.3 Yield Strength

Figure 17 shows that at operating temperatures, the yield strength of UO_2 varies by a factor of 2. A drop in yield strength causes additional plastic flow, and redistributes stresses/strains.

Reference 2 describes how the original version of ELESTRES accounted for the drop in yield strength. This has now been changed. For the current version of ELESTRES, special finite element equations were formulated for plastic flow during large changes in yield strength. Reference 7 gives the details and the resulting equations.

Figure 18 shows the results of a test case using this model. The test case simulates a cylinder under uniaxial tension in the plastic range, with a stress of 400 MPa and a strain of 0.46%. An increase in temperature then reduces the yield strength, which increases the plastic flow. The new strain is 0.63%. Figure 18 shows that the finite element method agrees well with the closed-form solution.

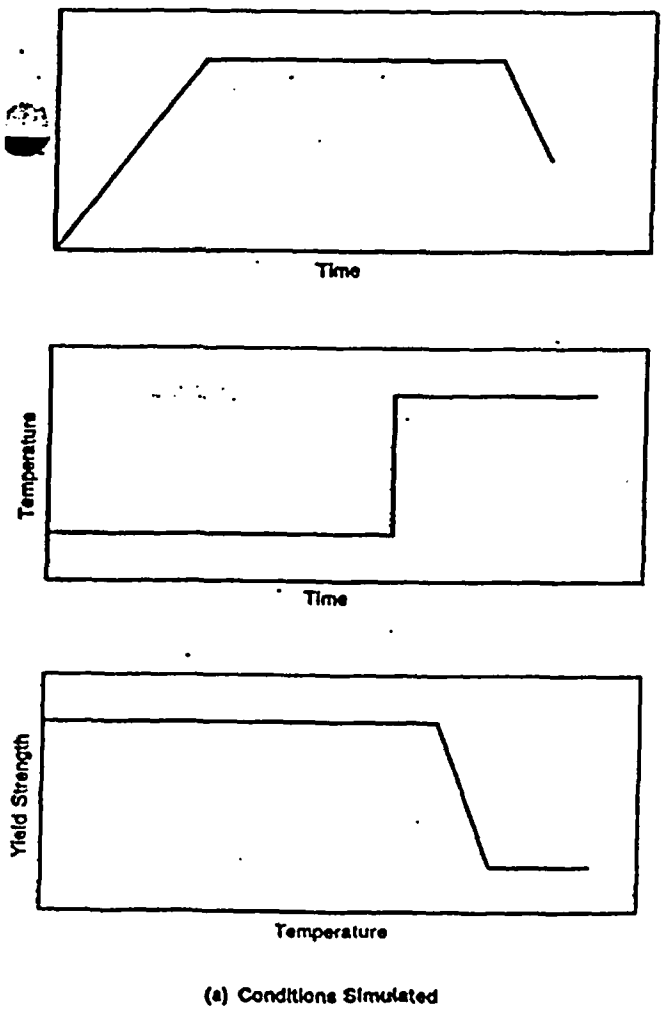

(a) Conditions Simulated

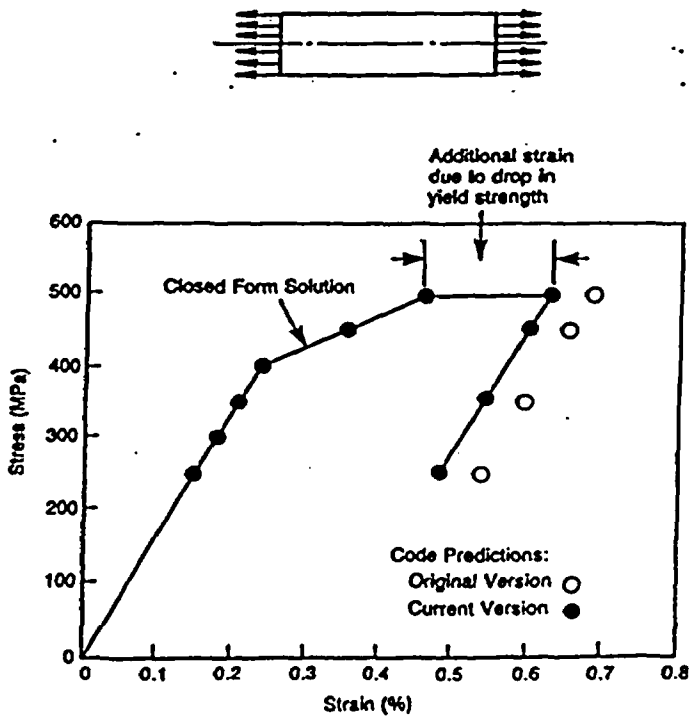

(b) Results

Figure 18 Strain Increase Due to Reduction in Yield Strength

5.4 Shapes of Finite Elements

The finite element method is used for calculating deformations, stresses, and strains, in pellets and in sheaths. Finite elements are available in two basic shapes: triangles, and rectangles. Rectangles are easier to use, because the nodes generally lie on grid-lines, and because the lines that connect the nodes are parallel to the coordinates axes. It is also easier to formulate the stiffness matrix of rectangular elements than of triangles; the difference is especially noticeable in elements of higher order. Below, we compare the accuracies of the two types of elements.

The stiffness matrix of a rectangular element can be generated by first dividing the rectangle into four triangles connected at the centroid of the rectangle, and then adding the stiffnesses of the four triangles [33]. Hence, for purposes of accuracy, a rectangular element is equivalent to four triangles assembled into a rectangular shape.

	Pattern	Error
1		O(1)
2		O(1)
3		O(1)
4		O(1)
5		O(1)
6		O(h)

	Pattern	Error
7		$O(h^2)$
8		$O(h^2)$
9		$O(h^2)$
10		$O(h^2)$
11		$O(h^2)$
12		$O(h^2)$

h represents the spacing between neighbouring nodes

$O(h)$ means that the discretization error is of order h

Figure 19 Convergence: Mesh Patterns [34]

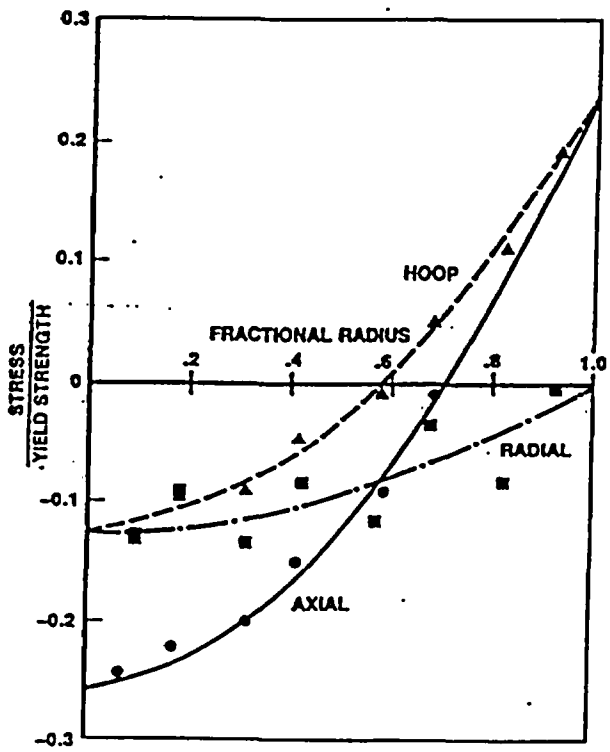

a) Rectangular Pattern of Triangles

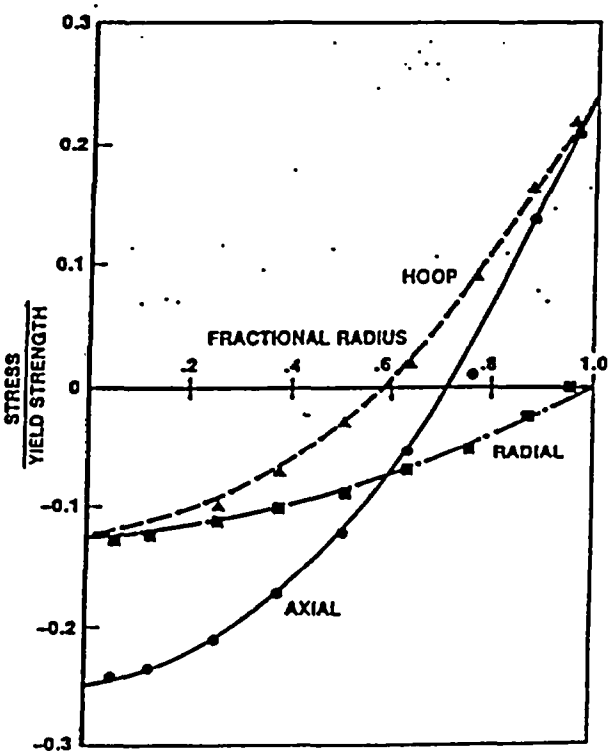

b) Hexagonal Pattern of Triangles

Figure 20 Thermal Stresses in a Cylinder : Analytical Solutions (Lines) vs. Finite Element Calculations (Points)

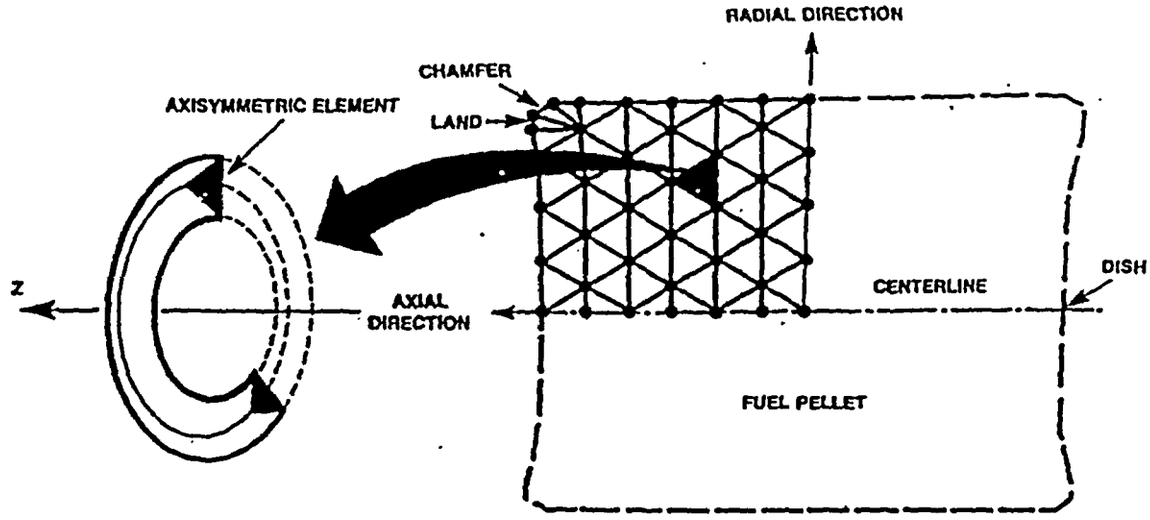

Figure 21 Finite Element Mesh in the Pellet

Udoguchi et. al. [34] have studied the accuracy of the solution vs the pattern into which individual finite elements are arranged. Figure 19 shows some of the patterns studied by Udoguchi et. al. for plane-stress problems. They used Taylor series to represent the finite-element equations, and determined the discretization error of the series as a function of spacing between nodes. They found that when triangular elements are arranged in a rectangular pattern, the solution converges slowly. Also, it always retains a residual error. However, if the triangular finite elements are assembled into a hexagonal pattern, the solution converges rapidly to the true solution. This occurs because the two patterns compensate differently for shear.

Finite elements of higher order can accelerate the convergences of both the triangular and the rectangular elements [33].

We checked if the theoretical results of Udoguchi et. al. have a significant effect on stresses in pellets. We modelled a solid cylinder experiencing a parabolic distribution of temperature along its radius. We calculated the axisymmetric stresses due to the temperature-gradient.

Figure 20a shows the calculated stresses when the elements were arranged in a rectangular pattern. Compared to the analytical solutions, the rectangular pattern, hence rectangular elements, provide reasonable predictions for hoop and axial stresses, but the axial stresses show large scatter. The hexagonal pattern, however, gives better predictions for all three components, and the scatter is negligible, see Figure 20b.

Triangular elements have another advantage: complex profiles can be more easily recreated by assembling triangles than by assembling rectangles.

For these reasons, ELESTRES uses triangular elements arranged in a hexagonal pattern.

5.5 Stresses

The dominant source of stresses on the sheath, is expansion and hourglassing of the pellet. In ELESTRES, the pellet is represented by 50-60 triangular finite elements assembled into a hexagonal pattern, see Figure 21. Reference 2 describes the details of this model.

During irradiation, the sheath develops primary and secondary stresses. The primary stresses depend on factors like: coolant pressure; fission gas pressure; and hydraulic drag; see Figure 22. The primary stresses are mainly in the hoop and in the axial directions. The stresses and strains are well into the plastic range: Hoop strains of ~1% have been measured.

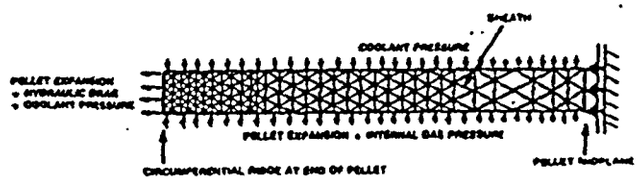

Figure 22 Loads on the Sheath, and a Finite Element Mesh

For normal values of element power, the pellet expands more than the available radial clearance between the sheath and the pellet. This leads to secondary stresses in the sheath. Because of hourglassing, the stresses are higher near the circumferential ridge than near the midplane of the pellet. This generates in the sheath, hoop, bending (axial), shear, and radial stresses. Additional secondary axial stresses arise from axial interaction between neighbouring pellets, and from axial interaction between the endcap and the stack of pellets. The secondary stresses relax rapidly due to creep.

For sheath stresses, the default option in ELESTRES uses [2] a simple force-balance in the hoop direction. These calculations consider: the coolant pressure, the internal gas pressure, and the interfacial pressure between the pellet and the sheath.

A more detailed study using the FEAST code showed [11] that near the ridge, the strains are highly multiaxial. The multiaxiality, however, makes a significant difference to the level of stresses. For example, if other components of stresses were not present, the hoop stress cannot exceed the uniaxial tensile yield strength. But because of multiaxiality, the maximum hoop stress can be significantly higher than the uniaxial tensile yield strength.

All components of stresses contribute to the damage of the sheath. For example, Reference 11 investigates the influence of multiaxiality, on the fatigue of the sheath, during power-cycling. The conclusion is that when the entire stress-system is applied on the sheath, the cycles to failure are half of those when only the hoop stress is applied.

For this reason, an option in ELESTRES now permits more accurate and detailed calculations of sheath stresses. When the option is activated, for example to calculate sheath stresses after a power-boost, ELESTRES creates and preserves pertinent data in a computer file. This data is then used by a more versatile stress-analysis code like FEAST [7]. The most important information in this file relates to the hourglassed shape of the pellet. Figure 4 shows the links among the codes. The following paragraphs describe the detailed calculation of sheath stresses.

The calculations using FEAST are multiaxial, axisymmetric, and elastic-plastic. They account for the axial variations in displacements/strains/stresses of the sheath, due to: pellet expansion and hourglassing; internal gas pressure; coolant pressure; and axial interactions.

Sheath stresses are calculated by solving simultaneously, the multiaxial classical equations describing the following fundamental laws of mechanics: equilibrium; compatibility; constitutive relations; yield criterion; and flow rule. Since the solution is obtained by using the FEAST code, these calculations are similar to those for pellet deformation [2]. Reference 7 gives a more detailed description of the methods of solution.

Figure 22 shows a typical mesh in the sheath. The sheath contains a finer mesh than the pellet; this reflects the need to know detailed local variations in the sheath. The mesh in the sheath is tied to the mesh of the pellet; this precludes the need for interpolations and extrapolations.

The study reported in Reference 11 showed that strains can change rapidly along the thickness of the sheath, and along its length. Because of the importance of stresses near the ridge, we use 5 nodes across the thickness at that location. Stresses are less critical near the midplane of the pellet, so 2 nodes are sufficient there. The comparatively coarse mesh near the midplane helps reduce computing-cost.

The transition from big to small elements is gradual; this prevents the larger elements from dwarfing the stiffnesses of neighbouring smaller elements. For maximum accuracy, the aspect ratio is kept close to 1. The sheath is usually represented by about 200 nodes, forming about 300 triangular finite elements in a hexagonal pattern. Our experience shows that this combination gives sufficient accuracy at low cost.

5.6 Creep of Sheath

Stresses lead to creep of the sheath. Anisotropy of the sheath plays an important role in the rate of creep. At 300-350°C, the rate of creep of Zircaloy can be calculated using the model by Hosbons, Coleman and Holt [35]. This model considers athermal and thermal creep due to changes in dislocation densities, and the effect of irradiation. Reference 1 describes the application of this model to ELESTRES.

For off-normal conditions, the temperature of the sheath may be higher than 350°C. Then, the above model is not adequate, and ELESTRES uses the model by Sills and Holt [36]. This model is applicable for temperatures above 350°C, and accounts for creep due to::

- thermal and athermal strains due to changes in dislocation densities,
- diffusional creep due to sliding at grain boundaries, and
- transformation strain due to expansion at the crystal lattice, during the transition of Zircaloy from α to β phase.

The rate of creep from the above three components depends on: temperatures; stresses; and microstructures of Zircaloy. Temperatures and stresses have already been discussed. The following paragraph summarizes the three major microstructural parameters considered in ELESTRES: recrystallization; fractions of α and β phases; and grain size.

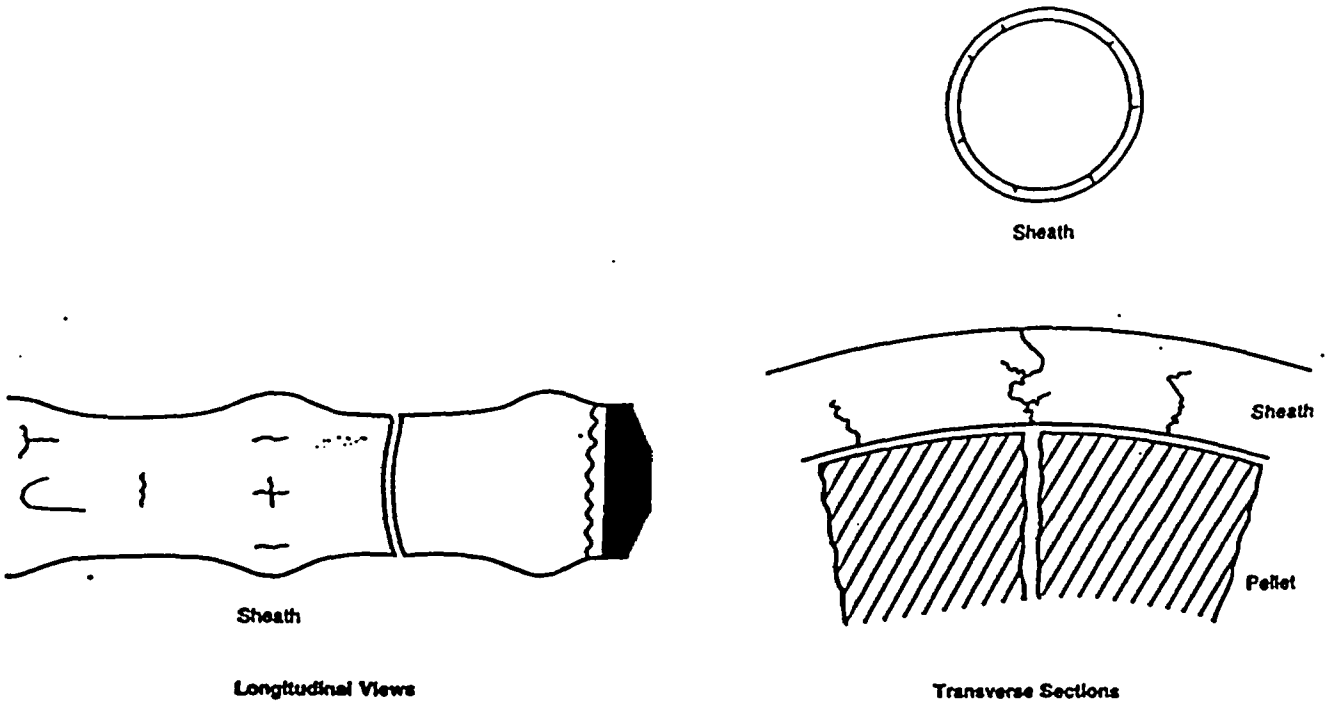

Figure 23 Examples of Possible Cracks in the Sheath of a Nuclear Fuel Element

Recrystallization, or annealing, occurs in Zircaloy above ~ 430°C. Within the old grains, nucleation and growth of recrystallized grains give areas with low densities of dislocations. These areas grow thermally, thus annealing the material. The rate of removal of dislocations is estimated from the empirical model by Sills and Holt [36]. The distribution of α and β phases depends on the temperature, and is obtained from the phase diagram. The size of grains is also a function of temperature. It is obtained from an empirical correlation based on microscopic examinations of fuel sheaths after heating to various temperatures. Further details of the creep model are available from Reference 36.

During creep calculations, ELESTRES continually updates the microstructure of Zircaloy, to reflect the temperature transient.

5.7 Stress Corrosion Cracking

The failure rate, about 0.1% in 500,000 bundles irradiated [1], is very low in current CANDU fuel, which contains a layer of CANLUB. In the past, however, fuel failures have been reported [37] at circumferential ridges, and related to stress corrosion cracking during power ramps. The initiation of the cracks can sometimes be assisted by delayed hydride/deuteride cracking. Some types of cracks have been reported previously [1, 37, 38], and shown schematically in Figure 23.

Stress corrosion cracking occurs when a large stress is maintained for a long time, simultaneously with high concentrations of corrodants (active species). Initiation of stress corrosion cracks is easier in the presence of suitably oriented platelets of zirconium hydrides (deuterides). Another way in which irradiation promotes stress corrosion cracking, is by embrittling the Zircaloy.

Fuel failures discussed in Reference 37 were eliminated from CANDU fuel by introducing a layer of CANLUB, which reduces the exposure of the sheath to fission products, and by changing to new fuel-management schemes that give low stresses in the sheath.

For stress corrosion cracking, ELESTRES uses an empirical correlation based on irradiations at Pickering, Douglas Point, and Chalk River. The probability of failure is calculated from:

- ramped power;
- change in power;
- burnup;
- dwell time at high power; and
- the presence of a protective layer of CANLUB at the inner surface of the sheath.

For this calculation, algebraic equations are used, based on the empirical correlations Fuelograms [37] and Fulomo.

6. PROPERTIES AND FEEDBACKS

6.1 Material Properties

The following properties of UO_2 and of Zircaloy, are used in ELESTRES: thermal conductivity; specific heat; coefficient of thermal expansion; Young's modulus; Poisson's ratio; yield strength; plastic modulus; creep rate; and stress for fracture. For use in ELESTRES, the values of these properties were obtained largely from the MATPRO data base [25]. Many of the properties depend strongly on local temperature, especially the diffusivity of gas in UO_2; the thermal conductivity of UO_2; the yield strength of UO_2; and the creep rates of UO_2 and Zircaloy.

For creep of UO_2, ELESTRES uses the equations suggested by Armstrong [39]. The rate of UO2 creep depends on: local temperature; local stresses; and local rate of heat generation. The strain rate can be high at operating conditions: At 1200°C and 100 MPa, the creep rate in UO_2 is 0.3% per day.

6.2 Feedbacks

Most of the preceding processes interact, and influence each other. For example, thermal expansion of the pellet increases the interfacial pressure between the sheath and the pellet, which lowers the temperature of the pellet, which reduces the amount of thermal expansion. Similarly, densification of UO_2 increases its thermal conductivity, which reduces the temperature, which slows further densification. Similar examples can be constructed for fission gas release, for sheath strain, and for internal pressure. ELESTRES accounts for the interdependence of these parameters.

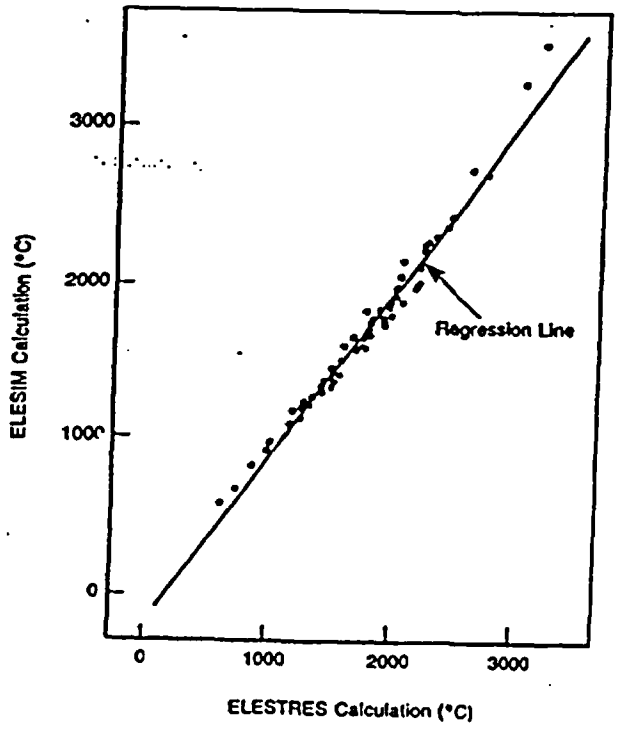

Figure 24 Temperatures at the Center of the Pellet

7. VALIDATION

Many of the physical processes are represented in ELESTRES by the same models as in ELESIM. The major difference is that the interactions among the sub-models are arranged slightly differently, and that some models are new in ELESTRES (e.g. hourglassing). Comparisons for about 80 irradiations show that, as expected, ELESTRES and ELESIM predict similar temperatures in the pellet, see Figure 24. Hence, previous validations of ELESIM also apply to ELESTRES, for processes that are driven largely by temperatures: UO_2 grain sizes [14], Figures 25 and 26; porosity [40], Figure 27; and fission gas release.

Figure 26 shows [14] the sizes of UO_2 grains across the pellet radius, in bundle 14672 irradiated at Pickering. The grain size is largely a function of time-at-temperature, and the figure reflects the influence of the parabolic temperature.

The trends shown in Figure 27 are due to a competition between volume-reduction due to densification, and volume increase due to swelling from unreleased fission products (solid and gaseous) in UO_2 grains and at grain boundaries:

- Center of the pellet: Densification is high. It is balanced by a moderate level of unreleased fission products.
- Fractional radius of 0.4: Densification is high. But gas release is low, giving high swelling due to unreleased fission products.
- Fractional radius of 0.7: Densification is high. The fission products are mostly in the UO2 matrix, where they do not contribute to swelling.
- Pellet surface: Temperature is low. There is neither densification, nor fission product swelling. The void volume in the pellet is near the as-fabricated value.

Reference 2 compared the predictions of ELESTRES, against irradiation measurements of fission gas release (15 irradiations), and of sheath strains at circumferential ridges (10 irradiations). The irradiations were done in experimental reactors at Chalk River Nuclear Laboratories, and in commercial reactors in Ontario, Canada. The data base covered element powers of 50-120 kW/m, and burnups of 1-300 MW.h/kgU.

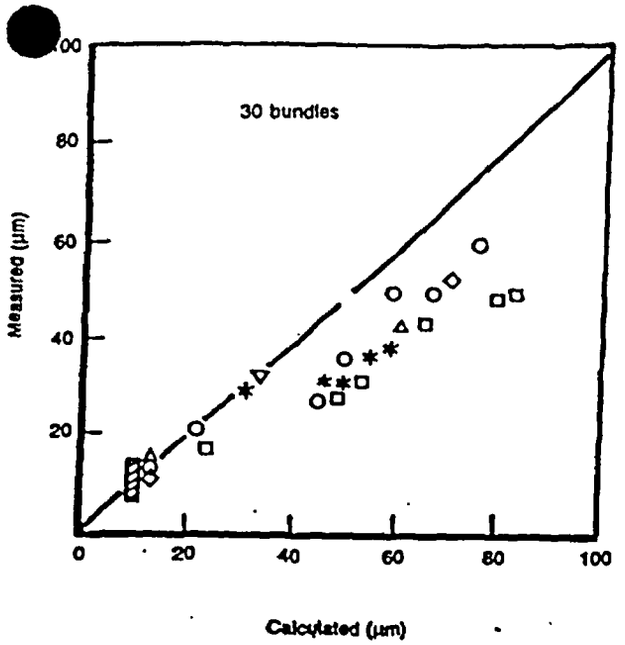

Figure 25 UO_2 Grain Sizes after Irradiation in Pickering [14]

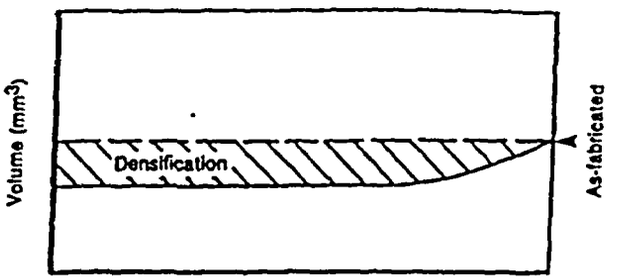

Volume Decrease due to Densification

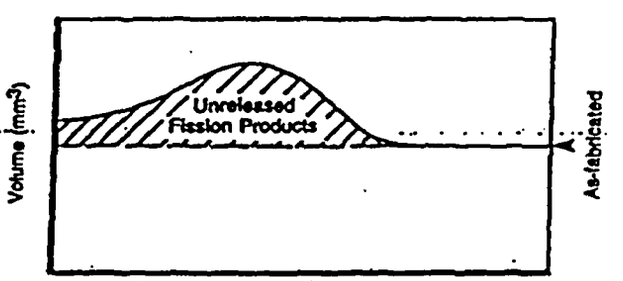

Volume Increase due to Unreleased Fission Products

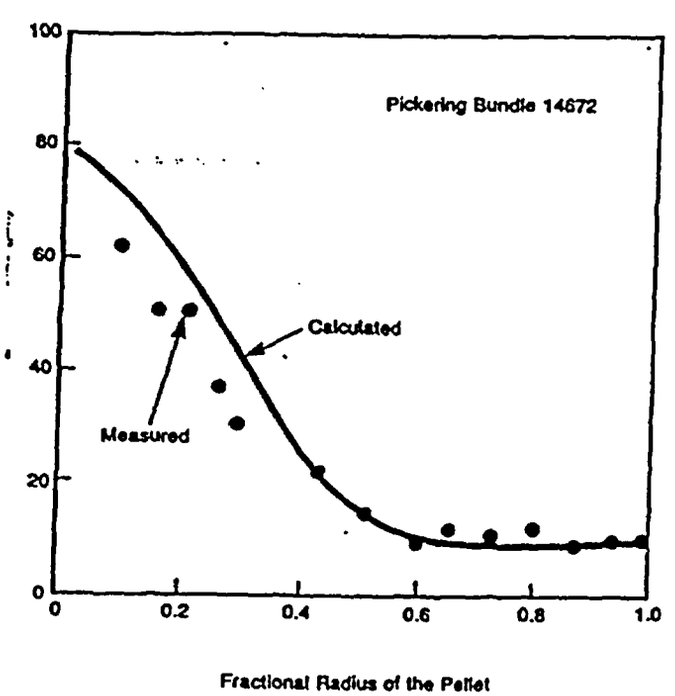

Figure 26 Measured and Calculated Values of UO_2 Grain Size Across a Section of a Pickering Element [14]

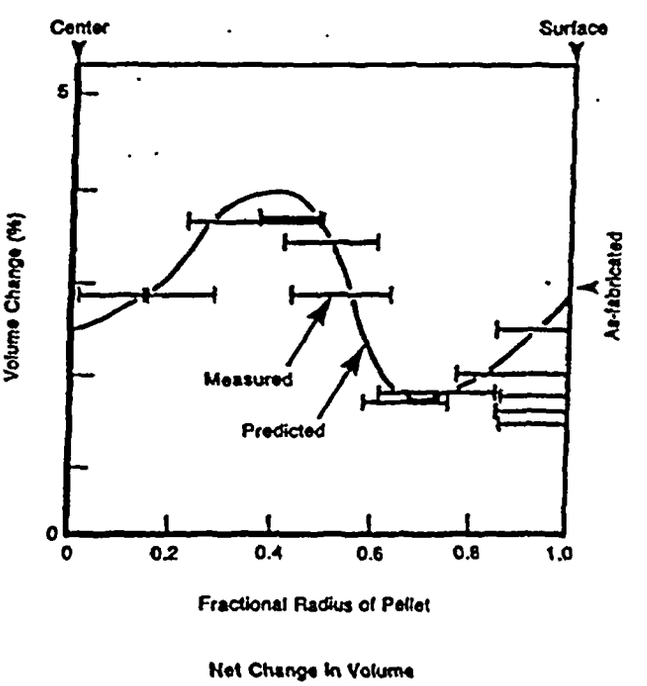

Figure 27 Change in UO_2 volume during irradiation (Pickering bundle 09794) [14]

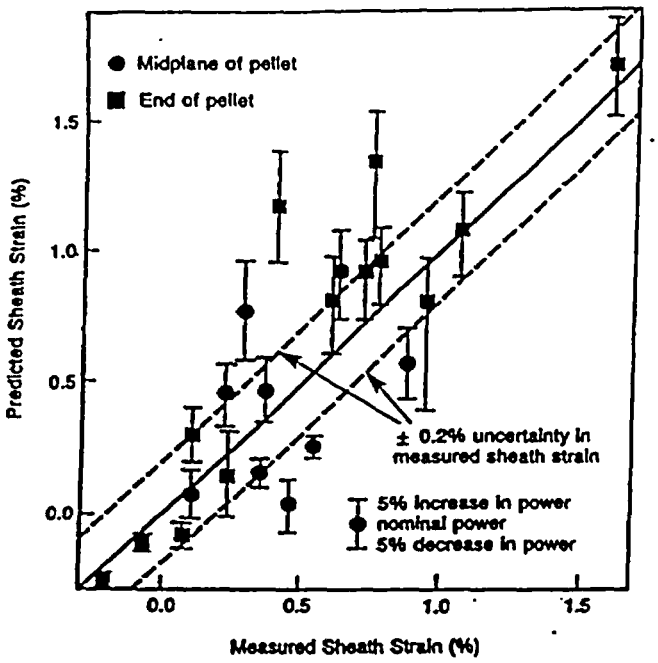

Figure 28 Final Values of Sheath Plastic Strains: Measured vs Predicted [2]

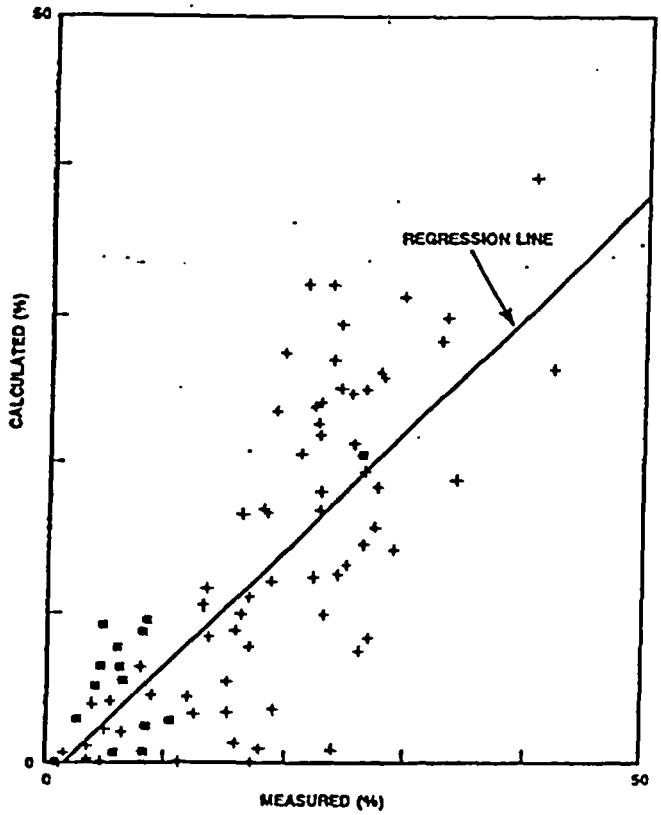

Figure 29 Fission Gas Release: Measurements vs. Predictions

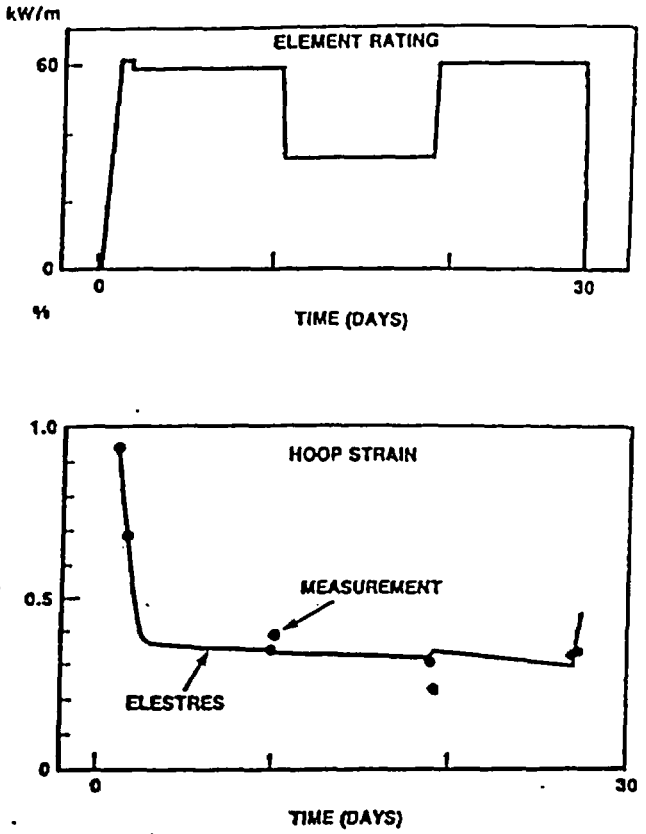

Figure 30 Hoop Strain at the Ridge in Element ABS: Measurements vs. ELESTRES

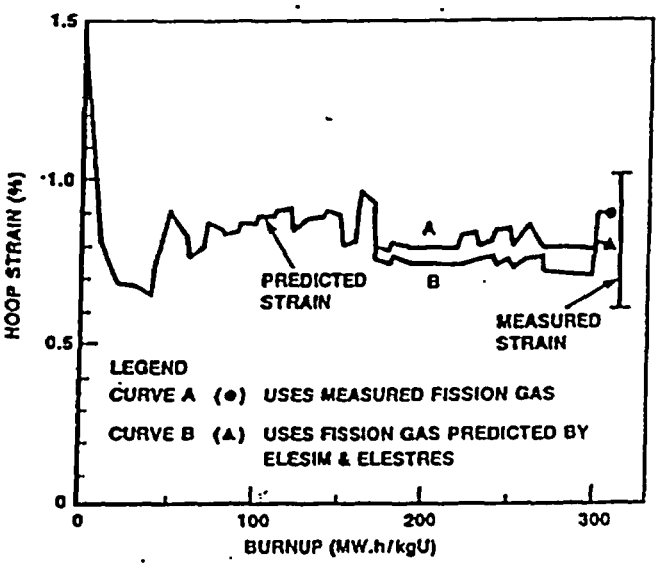

Figure 31 Plastic Hoop Strain at Circumferential Ridges in Bundle GB: Measurements vs. ELESTRES

On average, the predictions of ELESTRES differed from measurements, by 0.2 percentage points for hoop strain in the sheath, see Figure 28, and by 1.2 percentage points for percent release of fission gas.

The newer version of ELESTRES has now been compared against about 80 irradiations in experimental reactors and in commercial reactors. The predictions continue to show reasonable agreement with measurements of fission gas release, see Figure 29. The next two sections present two more validations of ELESTRES against irradiation data: element ABS and bundle GB.

7.1 Irradiation ABS

Element ABS was irradiated [41] for about one month at Chalk River Nuclear Laboratories, Canada. The power ranged from 30 to 60 kW/m. Hoop strain in the sheath was measured during the irradiation, using the In-Reactor Diameter Measuring Rig (IRDMR). Figure 30 shows the power history. It also compares the predictions of ELESTRES vs the measurements for hoop strains at the ridge, as a function of time. On average, the predictions compare well with measurements.

7.2 Irradiation GB

In this experiment [42], the outer element was irradiated at powers between 48 and [illegible] kW/m, to a burnup of 300 MW.h/kgU. Figure 31 shows that the predictions of ELESTRES are within the ranges of post-irradiation measurements, for hoop strains at circumferential ridges.

7.3 Sensitivity to Axial Nodes

Figure 32 illustrates how the results and the computing costs of ELESTRES are influenced by the size of the finite element mesh in the pellet. For irradiation GB, the figure shows the following parameters as a function of the number of axial nodes: fission gas release; permanent hoop strain at the ridge; and computing time for the Central Processor Unit (CPU) of a CDC/CYBER 175 computer.

Fission gas release is primarily a function of temperature, which does not depend much on the details of the finite element mesh: 100 radial nodes are always used for this finite difference calculation.

As expected, finer subdivision (more axial nodes) improves the calculations for hoop strains.

Also as expected, the computing cost increases with more axial nodes. When 3 axial nodes are used to simulate irradiation GB, ELESTRES requires 19 seconds of CPU time - similar to the 21 CPU seconds required by ELESIM for simulating the same irradiation. This modalization permits a hexagonal arrangement of finite elements, and is sufficient if the primary aim is to calculate fission gas release.

More detailed calculations of ridge strain require 7 axial nodes in the pellet, and 55 CPU seconds to simulate irradiation GB.

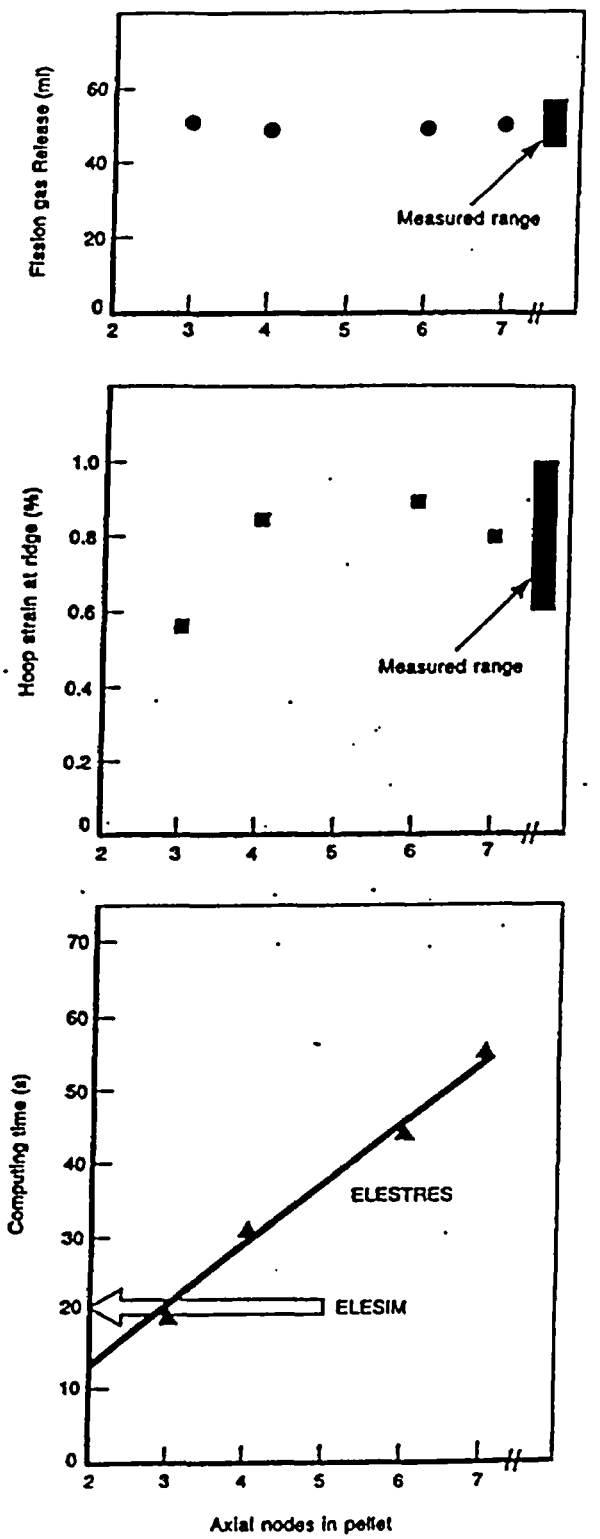

Figure 32 Sensitivity of ELESTRES Calculations, to Axial Subdivision of the Pellet

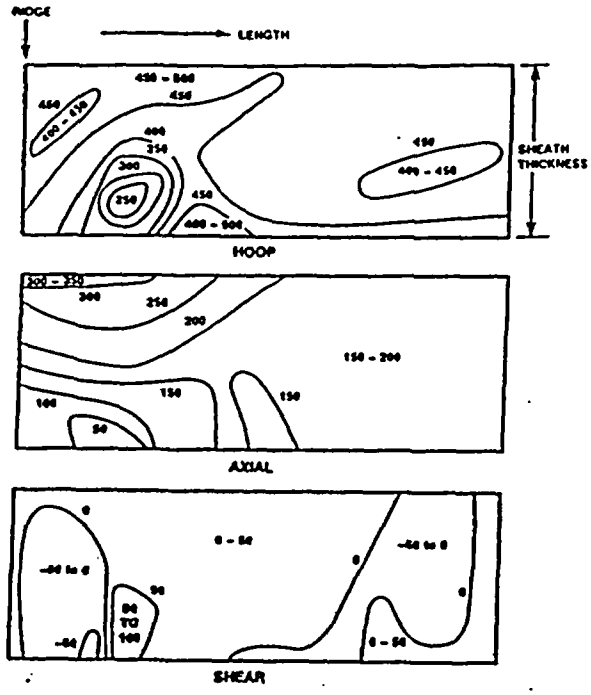

Figure 33 Elastic-Plastic Stresses (MPa) in the Sheath

8. ILLUSTRATIVE EXAMPLES

Reference 11 discusses some previous applications of ELESTRES. Below, two illustrative examples are presented. They do not necessarily represent conditions in fuel elements in experimental or in commercial CANDU reactors. Rather, the intent here is to demonstrate some capabilities of the code that are not apparent from the previous section on validation.

The first example demonstrates how ELESTRES and FEAST are linked to calculate the patterns of sheath stresses and strains in the sheath, for a power-boost of 40 kW/m at 140 MW.h/kgU. Figure 33 shows the results. The multiaxiality of stresses is clear. The axial stress shows sharp gradients across the thickness of the sheath. The shear stress shows significant variations along the length of the sheath. The maximum principal stress is 500 MPa. This, however, relaxes rapidly due to creep.

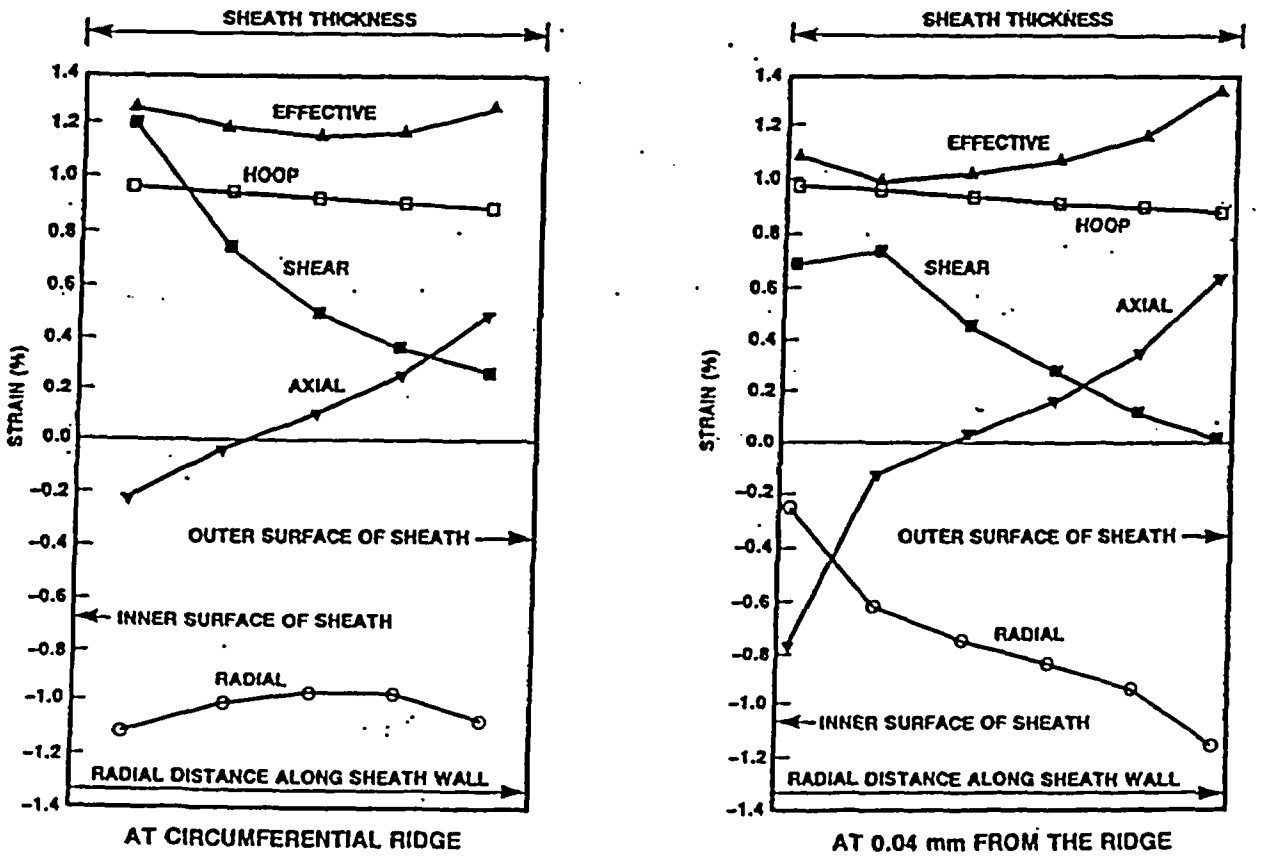

Figure 34 Strains across the Sheath Wall

Figure 34 shows the distribution of strains near a circumferential ridge, formed by a short-length-pellet, at a power of 56 kW/m at zero burnup. At the inner surface, the hoop and shear strains have similar magnitudes. At the outer surface, shear strains are low, but the axial strain is significant. The radial strain is compressive, but the absolute magnitude of peak radial strain is similar to that of hoop and shear strains. Thus, all four components contribute significantly to yield, creep, fatigue, and brittle fracture of the sheath.

The third illustrative example involves a Loss-of-Reactivity- Control accident (LORA). An excursion of power, at 80 MW.h/kgU, gradually increases the power by 18%. The coolant is maintained at full system pressure, but the overpower is assumed to cause dryout, which results in a low coefficient of heat transfer between the sheath and the coolant. Conservatively, it is assumed that the drypatch covers the entire element: all around the circumference, and all along the length. These assumptions are not realistic, but nevertheless used here to show that the code can be used for simulating transients such as LORAs. Figure 35 shows the prediction of ELESTRES, for sheath hoop strains near the ridge and near the midplane of the pellet. During the transient, the elevated temperatures in the pellet increase the hoop strain at the ridge. The ridge height also increases.

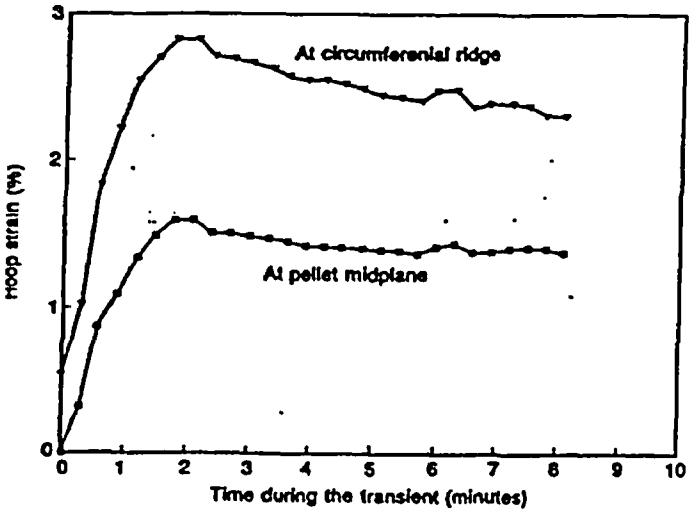

Figure 35 Sheath Strain during a Loss-of-Reactivity-Control Accident

9. SUMMARY AND CONCLUSIONS

(1) An improved version of ELESTRES has been developed for modelling the performance of nuclear fuel elements. The two-dimensional, axisymmetric calculations account for radial and axial variations.

(2) For given conditions of design and irradiation, the values of the following parameters can be calculated: temperatures, fission gas pressure, circumferential ridging, sheath stresses, and probability of failure due to stress corrosion cracking.

(3) Temperatures are calculated by a one-dimensional model. The standard finite difference method is used for steady-state temperatures, using 100 nodes across the radius. Transient temperatures use an implicit formulation and an iterative Newton-Raphson method.

(4) The finite element method is used for two-dimensional, axisymmetric calculations of displacements, stresses, and strains in the pellet. The pellet is represented by 40-50 finite elements. A link with FEAST permits detailed calculations of sheath stresses, using 200-300 finite elements. Elasticity, plasticity, creep and cracking are considered. Above 350°C, creep of Zircaloy is calculated from a model that considers diffusional creep and dislocation climb. This model accounts for changes in the microstructure of Zircaloy, such as grain size, and fraction of α and β phases. Special numerical techniques keep the computing time below 1 minute on a CDC/CYBER 175 computer.

(5) Triangular finite elements arranged in a hexagonal pattern, give better accuracy than rectangular elements.

(6) ELESTRES shows good agreement with measurements of fission gas release, from ~ 80 irradiations. The code also predicts well, sheath strains at circumferential ridges in experiments ABS and GB.

(7) By linking ELESTRES and FEAST, illustrative examples show a high degree of multiaxiality in sheath stresses and strains. The stresses/strains change rapidly with distance along the length of the sheath, and along the thickness.

ACKNOWLEDGEMENTS

The work reported in this document was funded partially by COG (CANDU Owners Group) R&D Program, as part of the 'Operating Fuel Technology' project: Work Package Number 2840. The author thanks the current members of 'Operating Fuel Technology' : Ontario Hydro, Atomic Energy of Canada Limited, Hydro Quebec, and New Brunswick Electric Power Corporation.

The author gratefully acknowledges the encouragement, support, and contributions of R. Sejnoha, M. Gacesa, D.R. Pendergast, D.B. Primeau, J.C. Wood, P.J. Fehrenbach, H.E. Sills, and J. Bunge. ELESIM, the starting point for ELESTRES, was developed largely by M.J.F. Notley. Special thanks to H.E. Sills (CRNL), for his permission to include in this paper, some of his unpublished results (Figures 24, 29), and to A. Banas for Figure 35.

REFERENCES

(1) P.T. Truant, "CANDU Reactor Experience: Fuel Performance", Sixth Annual Conference, Canadian Nuclear Society, 1985.

(2) H.H. Wong, E. Alp, W.R. Clendening, M. Tayal, L.R. Jones, "ELESTRES: A Finite Element Fuel Model for Normal Operating Conditions", Nuclear Technology, 57 (1982) 203-212.

(3) M. Tayal, "ELESTRES: Performance of Nuclear Fuel, Circumferential Ridging, and Multiaxial Elastic-Plastic Stresses in Sheaths", International Conference on CANDU Fuel, sponsored by the Canadian Nuclear Society, at Chalk River, Canada, 1986 October 6-8.

(4) R.D. Page, "Canadian Power Reactor Fuel", Atomic Energy of Canada Limited, Report AECL-5609, 1976.

(5) P.J. Fehrenbach, J.A. Walsworth, R.C. Spencer, W.R. Chase, R.D. Delaney, "In-Reactor LOCA Tests of Zircaloy-Sheathed UO_2 Fuel at Chalk River", Sixth Annual Conference of the Canadian Nuclear Society, Ottawa, Canada, 1985 June 3-4.

(6) C.E. Coleman, D. Mills, J. Van der Kurr, "Deformation Parameters of Neutron Irradiated Zircaloy-4 at 300°C", Canadian Metallurgical Quarterly, II (1972) 91-100.

(7) M. Tayal, "FEAST: A Two-Dimensional Non-Linear Finite Element Code for Calculating Stresses", Seventh Annual Conference, Canadian Nuclear Society, 1986.

(8) H.E. Sills, "ELOCA: Fuel Element Behaviour During High-Temperature Transients", Atomic Energy of Canada Limited, Report AECL-6357, 1979.

(9) M. Tayal, E. Mischkot, H.E. Sills, A.W.L. Segel, "ELOCA-A: A Code for Radial and Axial Behaviour of CANDU Fuel Elements at High Temperatures", Nuclear Technology, Volume 76, February 1987, p. 209-220.

(10) T.J. Carter, "Experimental Investigation of Various Pellet Geometries to Reduce Strains in Zirconium Alloy Cladding", Nuclear Technology, Vol. 45, September 1979, pages 166-176.

(11) M. Tayal, "Recent Uses of the Finite Element Method in Design/Analysis of CANDU Fuel", Sixth Annual Conference, Canadian Nuclear Society, 1985.

(12) M.J.F. Notley, "A Computer Program to Predict the Performance of UO_2 Fuel Elements", Nuclear Applications and Technology, Vol. 9, 1970 August, pages 195-204.

(13) M.J.F. Notley, "A Computer Code For Predicting the Performance of Nuclear Fuel Elements", Nuclear Technology, Vol. 44, August 1979, pages 445-450.

(14) M.J.F. Notley, I.J. Hastings, "Microstructure-Dependent Model for Fission Product Release and Swelling in UO_2 Fuel", Nuclear Engineering and Design, 56 (1980) 163-175.

(15) T. Nakajima, M. Ichikawa, Y. Ivano, K. Ito, H. Saito, K. Kashima, M. Kinoshita, T. Okubo, "FEMAXI-III: A Computer Code for the Analysis of Thermal and Mechanical Behaviour of Fuel Rods", Japan Atomic Energy Research Institute, Report JAERI-1298, December 1985.

(16) M. Tayal, D. Budney, "Load Increment Ratios in the Elastic-Plastic Analysis of Anisotropic Materials by the Variable-Stiffness Finite-Element Method", Journal of Strain Analysis, 11, 3, (1976), 150-153.

(17) J.E. Suich, H.C. Honeck, "The HAMMER System", Savannah River Laboratories, Report DP-1064, 1967.

(18) F.B. Campbell, L.R. Bourque, R. Deshaies, H.E. Sills, M.J.F. Notley, "In-Reactor Measurement of Fuel-to-Sheath Heat Transfer Coefficients Between UO_2 and Stainless Steel", Atomic Energy of Canada Limited, Report AECL-5400, 1977.

(19) M.H.M. Roshd and H.C. Chou, "The Analysis of Flux Peaking at Nuclear Fuel Bundle Ends Using PEAKEAN," Atomic Energy of Canada Limited, Report AECL-6174, April, 1978.

(20) J.J.H. Too, T.R. Hsu, A.W.H. Bertels, "FULMOD: An Inelastic Analysis Program to Predict the Operating Behaviour of CANDU Fuel Elements", published in: "Fuel Element Analysis", CONF-750617-17, American Society of Mechanical Engineers, New York, 1975, p. 23-35.

(21) J.J.H. Too, G.L. Rigby, H. Tamm, "Repeatable Boundary Conditions and their Application in the Analysis of a Complete CANDU Fuel Pin", Paper D1/8, Structural Mechanics in Reactor Technology, Transactions of the 4th International Conference, San Francisco, USA, 15-19 August 1977.

(22) I.J. Hastings, J.A. Scoberg, K. Mackenzie, "Grain Growth in UO_2: In-Reactor and Laboratory Testing", Atomic Energy of Canada Limited, Report AECL-6411 (1979).

(23) I.J. Hastings, "Structures in Irradiated UO_2 Fuel From Canadian Reactors", Atomic Energy of Canada Limited, Report AECL-MISC-249, 1983.

(24) A.J. Chapman, "Heat Transfer", McMillan Publishing Co., New York, 1974.

(25) D.L. Hagrman, G.A. Reymann, "MATPRO - Version 11: A Handbook of Material Properties for Use in The Analysis of Light Water Reactor Fuel Rod Behaviour", EG & G Idaho, Inc., Report NUREG/CR-0497, TREE-1280, R3, 1979.

(26) "Thermal Conductivity of Uranium Dioxide", Technical Report Series 59, p. 17-22, International Atomic Energy Agency, (1965).

(27) D.R. Olander, "Fundamental Aspects of Nuclear Reactor Fuel Elements", ERDA Report TID 26711 (1976).

(28) B.J. Buescher, R.O. Meyer, "Thermal Gradient Migration of Helium Bubbles in Uranium Dioxide", Journal of Nuclear Materials, 48 (1973) pp. 143-156.

(29) A.H. Booth, "A Method of Calculating Fission Gas Diffusion from UO_2 Fuel and Its Application to the X-2-f Loop Test", Atomic Energy of Canada Limited, Report AECL-496, 1957.

(30) "Background and Derivation of ANS 5.4 Standard Fission Product Release Model", compiled by Southern Science Applications, Inc.; American Nuclear Regulatory Commission, Report NUREG/CR-2507, 1982 January.

(31) I.J. Hastings, P.J. Fehrenbach, R.R. Hosbons, "Densification in Irradiated UO_2 Fuel", Communications of the American Ceramic Society, Vol. 67, No. 2, p C-24, 1984.

(32) J. Veeder, "Thermo-Elastic Expansion of Finite Cylinders", Atomic Energy of Canada Limited, Report AECL-2660, 1967.

(33) O.C. Zienkiewics, "The Finite Element Method in Structural and Continuum Mechanics", McGraw-Hill Book Company, 1967.

(34) T. Udoguchi, H. Okamura, T. Kano, Y. Nozue, "An Error Analysis of Various Finite Element Patterns", Bulletin of the Japanese Society of Mechanical Engineers, 16, 102 (1973) 1803-1813.

(35) R.R. Hosbons, C.E. Coleman, R.A. Holt, "Numerical Simulation of Tensile Behaviour of Nuclear Fuel Cladding Materials", Atomic Energy of Canada Limited, Report AECL-5245, 1975.

(36) H.E. Sills, R.A. Holt, "Predicting High Temperature Transient Deformation from Microstructural Models", ASTM STP 681 (1978) 325-341.

(37) W.J. Penn, R.K. Lo, J.C. Wood, "CANDU Fuel - Power Ramp Performance Criteria", Nuclear Technology, 34 (1977) 249.

(38) B. Cox, J.C. Wood, "Iodine Induced Cracking of Zircaloy Fuel Cladding - A Review", Atomic Energy of Canada Limited, Report AECL-4936, 1974.

(39) W. Armstrong, "Creep Deformation of Stoichiometric Uranium Oxide", J. Nucl. Mater., 7 (1962) 133.

(40) I.J. Hastings, M.J.F. Notley, D.H. Rose, "Irradiation - Induced Volume Changes in Commercial UO_2 Fuel: Comparison With Model Predictions", Journal of Nuclear Materials, Vol. 75, 1978, pages 301-303.

(41) P.J. Fehrenbach, P.A. Morel, "In-Reactor Measurement of Clad Strain: Effect of Power History", Atomic Energy of Canada Limited, Report AECL-6686, 1980.

(42) R.R. Meadowcroft, P.E. Hynes, H. Tayal, "Irradiation Behaviour of Prototype 37 Element CANDU Fuel at High Power", Bulletin of the American Ceramic Society, Vol. 57, No. 3, 1978, p. 361.

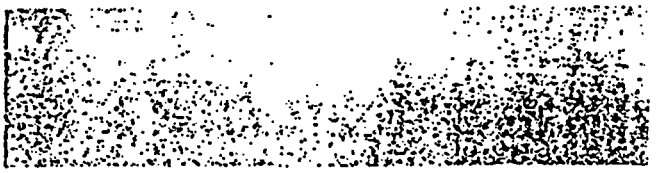

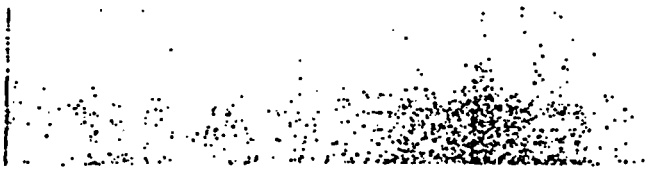

The International Standard Serial Number

ISSN 0067-0367

has been assigned to this series of reports.

To identify individual documents in the series we have assigned an AECL-number.

Please refer to the AECL-number when requesting additional copies of this document from

Scientific Document Distribution Office
Atomic Energy of Canada Limited
Chalk River, Ontario, Canada
K0J 1J0

Price $5.00 per copy

Le numéro de série standard international

ISSN 0067-0367

a été attribué à cette série de rapports.

Pour identifier les rapports individuels faisant partie de cette série nous leur avons attribué un numéro AECL-

Veuillez faire mention du numéro AECL- si vous demandez d'autres exemplaires de ce rapport au

Service de Distribution des Documents Officiels
L'Énergie Atomique du Canada, Limitée
Chalk River, Ontario, Canada
K0J 1J0

Prix $5.00 par exemplaire

PRINTED I
CANADA